



Synthesis, Characterization and Biological Activity of Transition Metals Schiff Base Complexes Derived from 4,6-Diacetylresorcinol and 1,8-Naphthalenediamine

Yasmin M. Ahmed¹ · Walaa H. Mahmoud¹ · M. M. Omar¹ · Gehad G. Mohamed¹

Received: 21 September 2020 / Accepted: 20 December 2020 / Published online: 10 February 2021
© The Author(s), under exclusive licence to Springer Science+Business Media, LLC part of Springer Nature 2021

Abstract

The tridentate Schiff base ligand was prepared via condensation of 4,6-diacetylresorcinol and 1,8-naphthalenediamine in 1:1 molar ratio using conventional method. Additionally, a new series of transition metal complexes of Cr(III), Mn(II), Fe(III), Co(II), Ni(II), Cu(II), Zn(II) and Cd(II) metal ions were prepared and fully characterized by elemental analysis, FT-IR, ¹H NMR, UV–vis, conductivity and magnetic susceptibility measurements and theoretically through density function theory (DFT). Spectral studies suggested that, the Schiff base coordinated to the metal ions through the azomethine N, N-amine and phenolic oxygen atoms. From the elemental, magnetic susceptibility and spectroscopic data, the complexes were suggested to have octahedral geometry. The Schiff base and its metal complexes were screened for their in vitro antimicrobial activities and showed that Cd(II), Cu(II) and Cr(III) complexes have high activity against *Escherichia coli*, while Ni(II) and Cd(II) complexes have the highest activity against *Bacillus Subtilis*, Co(II) complex has the highest activity against *Staphylococcus aureus* and Cd(II) complex has the highest activity against *Pseudomonas aeruginosa*. In addition, the molecular docking study was performed to explore the possible ways for binding to crystal structure of *Staphylococcus aureus* nucleoside diphosphate kinase complexed with ADP (PDB ID: 3Q8U).

Keywords Metal complexes · Schiff base ligand · Spectroscopic analysis · Microbial and anticancer activity · Molecular docking · Density functional theory (DFT)

1 Introduction

Schiff bases played a critical part in the development of coordination chemistry. Schiff base metal complexes have been researched widely because of their attractive chemical and physical properties in addition to their wide range of uses in numerous scientific areas [1]. Schiff bases have biological activity as anticancer and antibacterial where they characterized by an imine group –N=CH–, which helps to explain the mechanism of transamination and racemization reaction in biological system [2]. Imine complexes are immersed in the treatment of cancer drug resistance, and frequently tested as antimalarials. It also could be used for the immobilization of enzymes [3]. Additionally, Schiff base coordination

complexes are still of great importance because of their simple preparation, diverse chemical structures, wide applications such as biological modeling, catalysis, molecular magnets and material chemistry [4]. The published results have shown that these compounds possess effective role against bacteria and fungi which may be due to hetero atoms and/or azomethine linkage present in these compounds [5].

Transition metal complexes derived from Schiff bases had occupied an essential role in the development of coordination chemistry. Schiff base ligands are able to stabilize them in different oxidation states and to coordinate with many various metals, enabling the use of Schiff base metal complexes for a large range of useful catalytic transformations [6]. The bifunctional carbonyl compound; 4,6-diacetylresorcinol (DAR) serves as precursor for the building of tridentate ligands. Over the past few years, 4,6-diacetyl-resorcinol had also received much attention towards the biological applications as well as the coordination chemistry [7, 8]. 1,8-DAN is primarily used as intermediates in the production of

✉ Yasmin M. Ahmed
yassmine@sci.cu.edu.eg

¹ Chemistry Department, Faculty of Science, Cairo University, Giza 12613, Egypt

solvent dyes, such as C.I. solvent red 135, C.I. solvent orange 60 [https://issuu.com/nehapatilozone/docs/global_2.docx].

This work intentions to synthesize novel Schiff base ligand (H_2L) through the condensation of 4,6-diacetyl-resorcinol and 1,8-naphthalenediamine (H_2L). The metal complexes were prepared using 1:1 (M: L) molar ratio with metal ions like Cr(III), Mn(II), Fe(III), Co(II), Ni(II), Cu(II), Zn(II) and Cd(II). The structures of the ligand and its metal complexes were characterized by elemental analysis, FT-IR, 1H NMR, molar conductance measurements, electronic spectral study and thermal analysis. Docking studies were performed using MOE 2008 and its severe molecular docking software. The Schiff base ligand and its Zn(II) complex were completely optimized employing DFT based B3LYP method along with the LANL2DZ basis set. In order to incorporate the effect of the solvent around the molecule, the TD-DFT method (along with LANL2DZ: basic set) was employed. Anticancer and antibacterial abilities have evaluated [8].

2 Experimental

2.1 Materials and Reagents

All chemicals used were of the analytical reagent grade (AR) and of the highest purity accessible. The chemicals used involved 1,8-naphthalenediamine which was provided from Strem Chemicals Inc., 4,6-diacetyl resorcinol, $CrCl_3 \cdot 6H_2O$, $MnCl_2 \cdot 2H_2O$ and $FeCl_3 \cdot 6H_2O$ (Sigma-Aldrich), $NiCl_2 \cdot 6H_2O$, $CoCl_2 \cdot 6H_2O$, $CuCl_2 \cdot 2H_2O$ and $ZnCl_2$ (BDH) and $CdCl_2$ (Merck). Organic solvents consumed were ethyl alcohol (95%), methyl alcohol and N,N-dimethylformamide (DMF). Bidistilled water was usually getting through all preparations.

2.2 Solutions

1×10^{-3} M Stock solutions of the Schiff base ligand (H_2L) and also its metal complexes were prepared by dissolving an exactly weighed amount in DMF solvent. The conductivity then measured for the metal complexes solutions. Dilute solutions of the Schiff base ligand and its metal complexes (1×10^{-4} and 1×10^{-5} M) were prepared by accurate dilution from the previous prepared stock solutions for measuring their UV–vis spectra.

2.3 Solution of Anticancer Study

A fresh stock solution (1×10^{-3} M) of Schiff base ligand (0.12×10^{-2} g L^{-1}) was prepared in the suitable volume of DMF (90%). DMSO was used in cryopreservation of cells. RPMI-1640 medium was used. The medium was used

for culturing and keep of the human tumor cell line. The medium was contributed in a powder form. It was gotten ready as follows: 10.4 g of medium was weighed, mixed with 2 g of sodium bicarbonate, completed to 1 l with distilled water and shaken prudently until complete dissolution. The medium was then uncontaminated by filtration in a Millipore bacterial filter (0.22 μ m). The prepared medium was kept in a refrigerator (4 °C) and checked at methodical intervals for contamination. Before use, the medium was warmed at 37 °C in a water bath and supplemented with penicillin–streptomycin and FBS. Sodium bicarbonate was used for the preparation of RPMI-1640 medium. Isotonic trypan blue solution (0.05%) was prepared in normal saline and was used for feasibility counting. FBS (10%, heat inactivated at 56 °C for 30 min), 100 units/mL penicillin and 2 mg/mL streptomycin were used for the supplementation of RPMI-1640 medium prior to use. Trypsin (0.25×10^{-1} % w/v) was used for the picking of cells. Acetic acid (1% v/v) was used for dissolving unbound SRB dye. SRB (0.40%) dissolved in 1% acetic acid was used as a protein dye. A stock solution of trichloroacetic acid (50%) was prepared and stored. An amount of 50 μ L of the stock was added to 200 μ L of RPMI-1640 medium per well to yield a final concentration of 10% used for protein precipitation. Isopropanol (100%) and ethanol (70%) were used. Tris base (10 mM; pH 10.50) was used for SRB dye solubilization. Tris base (121.10 g) was dissolved in 1000 ml of distilled water and the pH was attuned using hydrochloric acid (2 M).

2.4 Instrumentation

Microanalyses of carbon, hydrogen and nitrogen were carried out at the Microanalytical Center, Cairo University, Egypt, using a CHNS-932 (LECO) Vario elemental analyzer. Analyses of the metals were controlled by dissolving the solid complexes in concentrated HNO_3 , and dissolving the remainder in deionized water. The metal content was carried out using inductively coupled plasma atomic absorption spectrometry (ICP-AES), Egyptian Petroleum Research Institute. Fourier transform infrared (FT-IR) spectra were recorded with a Perkin Elmer 1650 spectrophotometer ($400\text{--}4000\text{ cm}^{-1}$) as KBr pellets. 1H NMR spectra, as solutions in $DMSO-d_6$, were chronicled with a 300 MHz Varian-Oxford Mercury at room temperature using tetra-methylsilane as an interior standard. Mass spectra were chronicled using the electron ionization technique at 70 eV with an MS-5988 GS-MS Hewlett-Packard instrument at the Microanalytical Center, National Center for Research, Egypt. UV–vis spectra were acquired with a Shimadzu UVmini-1240 spectrophotometer. Molar conductivities of 10^{-3} M solutions of the solid complexes in DMF solvent were measured with a Jenway 4010 conductivity meter. Thermogravimetric (TG) and differential

thermogravimetric (DTG) analyses of the solid complexes were carried out from room temperature to 1000 °C using a Shimadzu TG-50H thermal analyzer. Antimicrobial measurements were carried out at the Microanalytical Center, Cairo University, Egypt. Anticancer activity experiments were performed at the National Cancer Institute, Cancer Biology Department, Pharmacology Department, Cairo University. The optical density (OD) of each in good form was measured spectrophotometrically at 564 nm with an ELIZA microplate reader (Meter tech. R960, USA) [8, 16].

2.5 Synthesis of Schiff Base Ligand

The Novel Schiff base ligand (H_2L) was synthesized via condensation of 4,6-diacetylresorcinol (4,6-DAR) with 1,8-naphthalenediamine. A solution of 1,8-naphthalenediamine (15.2 mmol, 2.4 g) dissolved in ethanol was added dropwise to 4,6-DAR (15.4 mmol, 3 g) dissolved in DMF. The resulting mixture was stirred in reflux for about 4–5 h, through which brown solid compound was separated. It was filtered, washed, recrystallized from diethyl ether and dried in vacuum (Scheme 1).

Yield 89%; m.p. 96 °C; brown solid. Anal. Calcd for $C_{20}H_{18}N_2O_3$ (%): C, 71.72; H, 5.38; N, 8.36. Found (%): C, 71.59; H, 5.26; N, 8.30, FT-IR (cm^{-1}): phenolic $\nu(OH)$ 3402, carbonyl $\nu(C=O)$ 1637, azomethine $\nu(C=N)$ 1590, (NH_2) bending 661. 1H NMR (300 MHz, DMSO- d_6 , δ , ppm): 7.05–6.39 (m, 6H, Ar-H(naph)), 8.4 (s, 2H (benzene)), 12.22 (s, H, OH^a), 9.83 (s, H, OH^b). 5.45 (s, 2H, NH_2) 2.65 (s, 6 H (methyl)). λ_{max} (nm): 233 and 276 ($\pi-\pi^*$) and 324 ($n-\pi^*$).

2.6 Synthesis of Metal Complexes

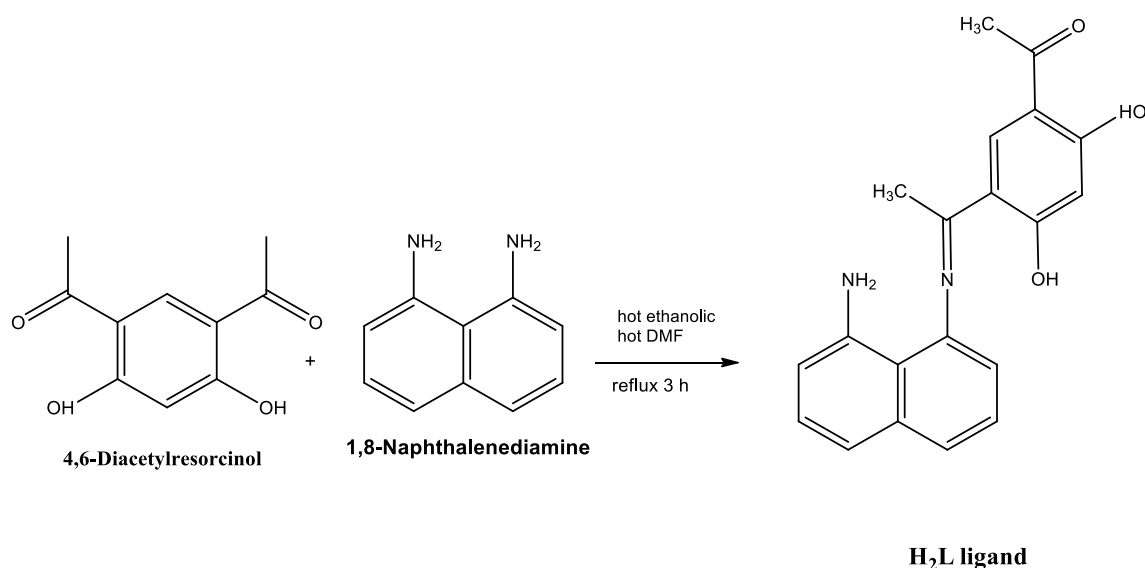
Complexes of H_2L with Cr(III), Mn(II), Fe(III), Co(II), Ni(II), Cu(II), Zn(II) and Cd(II) metal ions were prepared through reaction of 1:1 molar mixture of warm ethanolic solution (60 °C) of the suitable metal chloride (0.90 mmol) and H_2L (0.3 g, 0.90 mmol). The resulting mixture was stirred in reflux for 1 h at which the complexes precipitated. They were accumulated by filtration and purified by washing numerous times with diethyl ether.

2.6.1 $[Cr(H_2L)(H_2O)Cl_2]Cl \cdot 6H_2O$

Yield 87%; black solid, m.p. 198 °C. Anal. Calcd for $Cr(C_{20}H_{32}Cl_3N_2O_{10})$ (%): C, 38.78; H, 5.17; N, 4.52; Cr, 8.40. Found (%): C, 38.18; H, 5.13; N, 4.42; Cr, 8.34. FT-IR (cm^{-1}): phenolic $\nu(OH)$ 3430, carbonyl $\nu(C=O)$ 1638, azomethine $\nu(C=N)$ 1596, $\nu(H_2O)$ stretching bands of coordinated water 955 and 893, NH_2 bending 695, $\nu(M-O)$ 566, $\nu(M-N)$ 450. λ_{max} (nm): 227 and 277 ($\pi-\pi^*$) and 316 ($n-\pi^*$). μ_{eff} 3.98 B.M., Λ_m 57.80 $\Omega^{-1} mol^{-1} cm^2$.

2.6.2 $[Mn(H_2L)(H_2O)_2Cl]Cl \cdot 4H_2O$

Yield 80%; dark brown solid, m.p. > 300 °C. Anal. Calcd for $Mn(C_{20}H_{30}Cl_2N_2O_9)$ (%): C, 42.22; H, 5.29; N, 4.93; Mn, 9.68. Found (%): C, 42.16; H, 5.16; N, 4.83; Mn, 9.30. FT-IR (cm^{-1}): phenolic $\nu(OH)$ 3498, carbonyl $\nu(C=O)$ 1644, azomethine $\nu(C=N)$ 1600, $\nu(H_2O)$ stretching bands of coordinated water 953 and 880 NH_2 bending 668, $\nu(M-O)$ 567, $\nu(M-N)$ 482. λ_{max} (nm): 226 and 273 ($\pi-\pi^*$) and 323 ($n-\pi^*$). μ_{eff} 5.64 B.M., Λ_m 60.10 $\Omega^{-1} mol^{-1} cm^2$.



Scheme 1 Synthesis of Novel Schiff base ligand (H_2L)

2.6.3 [Fe(H₂L)(H₂O)₃]Cl₃·H₂O

Yield 83%; brown solid, m.p. 188 °C. Anal. Calcd for Fe(C₂₀H₂₆Cl₃N₂O₇) (%): C, 42.19; H, 4.57; N, 4.92; Fe, 9.84. Found (%): C, 41.89; H, 4.40; N, 4.69; Fe, 9.84. FT-IR (cm⁻¹): phenolic ν(OH) 3394, carbonyl ν(C=O) 1639, azomethine ν(C=N) 1560, ν(H₂O) stretching bands of coordinated water 958 and 890, NH₂ bending 697, ν(M–O) 506, ν(M–N) 454. λ_{max} (nm): 223 (π–π*). μ_{eff} 5.33 B.M., Λ_m 139.5 Ω⁻¹ mol⁻¹ cm².

2.6.4 [Co(H₂L)(H₂O)₂Cl]Cl·4H₂O

Yield 86%; black solid, m.p. > 300 °C. Anal. Calcd for Co(C₂₀H₃₀Cl₂N₂O₉) (%): C, 41.93; H, 5.24; N, 4.89; Co, 10.30. Found (%): C, 41.93; H, 4.96; N, 4.87; Co, 10.23. FT-IR (cm⁻¹): phenolic ν(OH) 3752, carbonyl ν(C=O) 1631, azomethine ν(C=N) 1580, ν(H₂O) stretching bands of coordinated water 955 and 829, NH₂ bending 620, ν(M–O) 577, ν(M–N) 468. λ_{max} (nm): 226(π–π*). μ_{eff} 4.89 B.M., Λ_m 73.8Ω⁻¹ mol⁻¹ cm².

2.6.5 [Ni(H₂L)(H₂O)₂Cl]Cl·6H₂O

Yield 80%; black solid, m.p. > 300 °C. Anal. Calcd for Ni(C₂₀H₃₄Cl₂N₂O₁₁) (%): C, 39.45; H, 5.59; N, 4.60; Ni, 9.70. Found (%): C, 38.95; H, 5.37; N, 4.45; Ni, 9.61. FT-IR (cm⁻¹): phenolic ν(OH) 3383, carbonyl ν(C=O) 1646, azomethine ν(C=N) 1598, ν(H₂O) stretching bands of coordinated water 955 and 894, NH₂ bending 654, ν(M–O) 572, ν(M–N) 459. λ_{max} (nm): 227 (π–π*). μ_{eff} 3.11 B.M., Λ_m 56.60 Ω⁻¹ mol⁻¹ cm².

2.6.6 [Cu(H₂L)(H₂O)₂Cl]Cl·5H₂O

Yield 84%; yellowish brown solid, m.p. 271 °C. Anal. Calcd for Cu (C₂₀H₃₂Cl₂N₂O₁₀) (%): C, 40.34; H, 5.38; N, 4.71; Cu, 10.68. Found (%): C, 40.04; H, 5.31; N, 4.63; Cu, 10.48. FT-IR (cm⁻¹): phenolic ν(OH) 3433, carbonyl ν(C=O) 1634, azomethine ν(C=N) 1562, ν(H₂O) stretching bands of coordinated water 940 and 900, NH₂ bending 654, ν(M–O) 593, ν(M–N) 460. λ_{max} (nm): 255 (π–π*). μ_{eff} 2.09 B.M., Λ_m 52.00 Ω⁻¹ mol⁻¹ cm².

2.6.7 [Zn(H₂L)(H₂O) Cl₂]3H₂O

Yield 80%; black solid, m.p. 200 °C. Anal. Calcd for Zn (C₂₀H₂₆Cl₂N₂O₇) (%): C, 44.25; H, 4.80; N, 5.16; Zn, 11.98. Found (%): C, 44.15; H, 4.59; N, 4.97; Zn, 11.83. FT-IR (cm⁻¹): phenolic ν(OH) 3445, carbonyl ν(C=O) 1631, azomethine ν(C=N) 1591, ν(H₂O) stretching bands of coordinated water 956 and 894, NH₂ bending 658, ν(M–O) 547, ν(M–N) 488. ¹H NMR (300 MHz, DMSO-d₆, δ, ppm):

7.12–6.23 (m, 6H, Ar–H(naph)) 8.40 (s, 1H (benzene)) 7.95 (s, 1H (benzene)) 12.23 (s, H, OH^a) 10.24 (s, H, OH^b) 5.38 (s, 2H, NH₂) 2.89 (s, 6 H (methyl)). λ_{max} (nm): 226 (π–π*), 324 (n–π*). μ_{eff} diamagnetic, Λ_m 15.50 Ω⁻¹ mol⁻¹ cm².

2.6.8 [Cd(H₂L)(H₂O) Cl₂]

Yield 85%; reddish brown solid, m.p. 186 °C. Anal. Calcd for Cd (C₂₀H₂₀Cl₂N₂O₄) (%): C, 44.71; H, 3.73; N, 5.23; Cd, 20.98. Found (%): C, 44.23; H, 3.51; N, 5.11; Cd, 20.33. FT-IR (cm⁻¹): phenolic ν(OH) 3376, carbonyl ν(C=O) 1639, azomethine ν(C=N) 1595, ν(H₂O) stretching bands of coordinated water 955 and 891, NH₂ bending 653, ν(M–O) 587, ν(M–N) 480. ¹H NMR (300 MHz, DMSO-d₆, δ, ppm): 7.15–6.24 (m, 6H, Ar–H(naph)), 8.41 (s, 1H (benzene)), 7.80 (s, 1H (benzene)), 12.21 (s, 1H, OH^a), 9.92 (s, H, OH^b), 5.40 (s, 2H, NH₂), 2.88 (s, 6 H (methyl)). λ_{max} (nm): 227 and 277 (π–π*), 316 (n–π*). μ_{eff} diamagnetic, Λ_m 1.00 Ω⁻¹ mol⁻¹ cm².

2.7 Spectrophotometric Studies

The absorption spectra were recorded for 1 × 10⁻⁴ and 1 × 10⁻⁵ M solutions of the Schiff base ligand and its metal complexes in DMF solvent, except for Cu(II) complex that had a concentration of 10⁻⁴ M. The spectra were scanned within the wavelength range from 200 to 700 nm [9].

2.8 Pharmacology

2.8.1 Antibacterial Activities

Antimicrobial activity of the tested samples was determined by a modified Kirby-Bauer disc diffusion method [10]. Briefly, 100 μl of the test bacteria were grown in 10 ml of fresh media until they reached a count of approximately 10⁸ cells/ml for bacteria [11]. 100 μl of microbial suspension was spread onto agar plates corresponding to the broth in which they were maintained. Isolated colonies of each organism that may be playing a pathogenic part should be selected from primary agar plates and tested for susceptibility by disc diffusion method [12]. Plates inoculated Gram (+) bacteria as *Staphylococcus aureus* and *Bacillus subtilis*; Gram (–) bacteria as *Escherichia coli* and *Pseudomonas aeruginosa*. They were incubated at 35–37 °C for 24–48 h and then the diameters of the inhibition zones were calculated in millimeters [10].

Standard discs of amikacin (Antibacterial agent), served as positive controls for antimicrobial activity but filter discs impregnated with 10 μl of solvent (distilled water, chloroform, DMSO) were used as a negative control. Blank paper disks (Schleicher & Schuell, Spain) with a diameter of 8.0 mm were impregnated 10 μl of tested concentration

of the stock solutions (20 mg/ml). When a filter paper disc impregnated with a tested chemical is placed on agar the chemical will diffuse from the disc into the agar. This diffusion will place the chemical in the agar only around the disc. The solubility of the chemical and its molecular size will determine the size of the area of chemical infiltration around the disc. If an organism is placed on the agar it will not grow in the area around the disc if it is susceptible to the chemical. This area of no growth around the disc is known as a “Zone of inhibition” or “Clear zone”. For the disc diffusion, the zone diameters were measured with slipping calipers of the National Committee for Clinical Laboratory Standards. Agar-based methods such as E-test and disk diffusion can be good alternatives because they are easier and more rapidly than broth-based methods [13, 14].

2.8.2 Anticancer Activity

Potential cytotoxicity of the compounds was tested via the method of Skehan and Storeng [15]. Cells were plated in 96-multiwell plate (104 cells/well) for 24 h before treatment using the compounds to let attachment of cell to the wall of the plate. Different concentrations of the compounds under investigation (0, 5, 12.5, 25, 50 and 100 µg/ml) were added to the cell monolayer and triplicate wells were prepared for each individual dose. The monolayer cells were kept warm with the compounds for 48 h at 37 °C and in 5% CO₂ atmosphere. After 48 h, cells were fixed, washed and stained with SRB stain. Excess stain was washed by acetic acid and attached stain was recovered with tris-EDTA buffer. The optical density (O.D.) of each well was measured spectrophotometrically at 564 nm with an ELIZA microplate reader, the mean background absorbance was automatically deducted and mean values of each drug concentration was calculated. The relation between drug concentration and surviving fraction is plotted to obtain the survival curve of breast tumor cell line for each compound [15, 16].

The percentage of cell survival was calculated as follows:

$$\text{Survival fraction} = \frac{\text{O.D. (treated cells)}}{\text{O.D. (control cells)}}$$

The IC₅₀ values (the concentrations of the Schiff base ligand (H₂L) or its metal complexes required to produce 50% inhibition of cell growth).

2.9 Computational Methodology

Gaussian09 suite of program was used for the electronic structure calculations of H₂L and Zn(II) complex. DFT based B3LYP method along using the LANL2DZ basis set were employed for full optimization. In order to incorporate the effect of the solvent around the molecule, the TD-DFT

method (along with LANL2DZ basic set) was used to estimate the electronic absorption spectra of the ligand and its zinc(II) complex. The contribution of molecular orbital on HOMO and LUMO were also calculated.

2.10 Molecular Docking

To find out the achievable binding modes of the best active compounds against Crystal structure of *Staphylococcus aureus* nucleoside diphosphate kinase complexed with ADP (PDB ID: 3Q8U), molecular docking studies were performed via MOE2008 software. It is rigid molecular docking software and is an interactive molecular graphics program for calculating and displaying feasible docking modes of a receptor and ligand and complex molecules. It necessitates the ligand and the receptor as input in PDB format. The amino acid chain was kept and the water molecules and co-crystallized ligands and chloride ions in out sphere were removed. The structure of ligand in PDB file format was created by Gaussian09 software. Crystal structure of *Staphylococcus aureus* nucleoside diphosphate kinase complexed with ADP (PDB ID: 3Q8U) was downloaded from the protein data bank (<http://www.rcsb.org/pdb>) [16].

3 Results and Discussion

3.1 Elemental Analysis

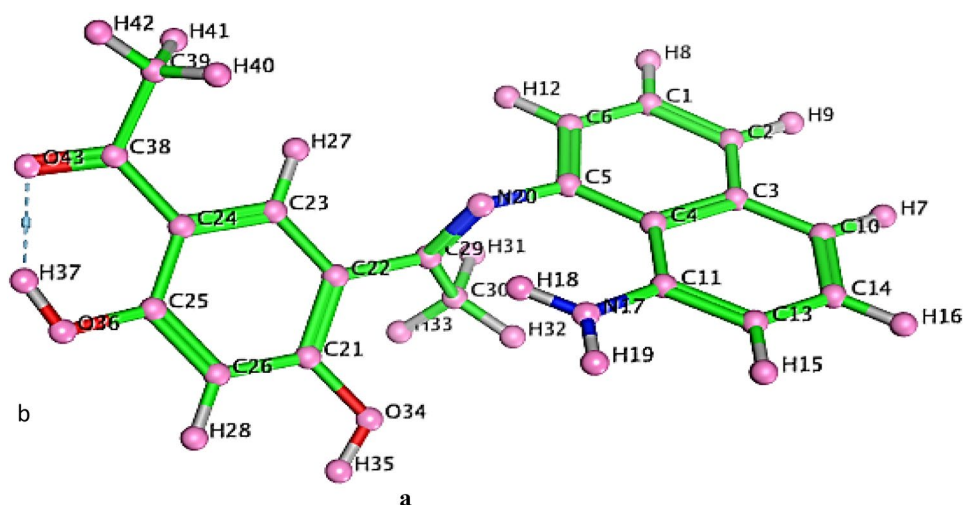
The synthesized Schiff base ligand (H₂L), namely [1-(5-(1-((8-aminonaphthalen-1-yl)imino)ethyl)-2,4-dihydroxyphenyl)ethanone] was a brown solid and stable at room temperature. It was soluble in ethanol. The results obtained were in good agreement with those calculated for the suggested formula. The structure of the Schiff base ligand under study was shown in Fig. 1 which also illuminating the intra molecular hydrogen bonding.

Metal complexes of H₂L ligand were synthesized through the reaction of ethanolic solutions of Schiff base and each metal salt in 1:1 ratio and they had the composition of MH₂L type. The results of experimental elemental analysis of H₂L and its complexes were to a large degree in agreement with the theoretical calculations.

3.2 Mass Spectral Study

The full scan mass spectra of ligand, Fe(III), Cr(III) and Ni(II) complexes were shown in Fig. 2. The ligand mass spectrum exhibited a molecular ion peak at m/z = 334.36 amu equivalent to [M]⁺, which confirmed the proposed formula [C₂₀H₁₈N₂O₃]⁺. The intensity of these peaks gave an idea of calculated value at 334.39 amu.

Fig. 1 Structure of Schiff base ligand (H_2L) illustrating the intra molecular hydrogen bonding



The mass spectrum of Cr(III) complex revealed a molecular ion peak at $m/z = 618.36$ amu which was concurrent with the calculated weight of 618.39 amu. This result confirmed the stoichiometry of this complex as being of $[MH_2L]$ type. On the other hand, the peak of the parent ligand in the mass spectrum of the Cr(III) complex appeared at m/z 334.11 amu. The full scan mass spectra of ligand and Cr(III) complex were shown in Fig. 2.

The mass spectrum of Ni(II) complex revealed a molecular ion peak at $m/z = 548.96$ amu which was concurrent with the calculated molecular weight of 549.39 amu. This result confirmed the stoichiometry of this complex as being of $[MH_2L]$ type. On the other hand, the peak of the parent ligand in the mass spectrum of the Ni(II) complex appeared at m/z 334.67 amu.

The mass spectrum of Fe(III) complex revealed a molecular ion peak at $m/z = 568.48$ amu which was concurrent with the calculated molecular weight of 568.89 amu. This result showed expected m/z values for molecular ion peak and peaks of corresponding fragments of Fe(III) complex (Fig. 3).

3.3 FT-IR Spectral Study

The characteristic infrared vibrational frequencies of the free ligand showed broad band at 3402 cm^{-1} attributed to the stretching frequency of $\nu(NH_2)$ and/or the phenolic group; $\nu(OH)$, band at 1637 cm^{-1} attributed to the stretching frequency of keto carbonyl group, band at 1590 cm^{-1} ascribed to the stretching frequency of $-C=N-$ and band at 661 cm^{-1} attributed to NH_2 bending vibration [7, 18].

IR spectra of the complexes were recorded to confirm their structures. The vibrational frequencies and their tentative delegations for H_2L ligand and its transition metal complexes can justify by comparison of the IR spectra of the metal complexes with those of the free ligand. The data

revealed that all complexes showed broad bands in the range $3376\text{--}3452\text{ cm}^{-1}$ which may be recognized to the stretching frequency of $\nu(NH_2)$ and/or the phenolic group; $\nu(OH)$, a water molecules related with the complexes which may be further confirmed by 1H NMR and thermal analyses [7, 17, 18].

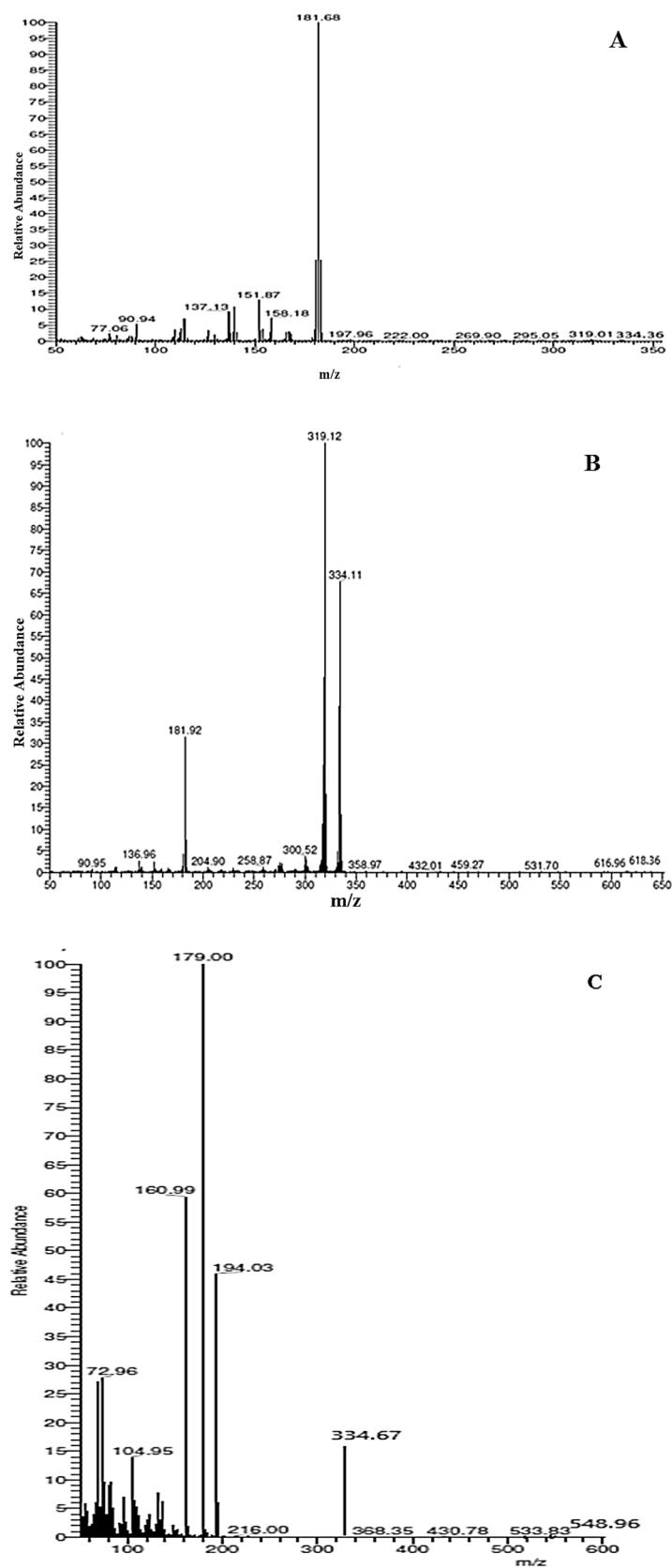
The band attributable to $\nu(C=N)$ azomethine stretching vibration of ligand that appeared at 1590 cm^{-1} , was shifted in complexes and appeared at $1560\text{--}1600\text{ cm}^{-1}$ which can attribute to coordination of azomethine nitrogen to metal ions [6, 19, 20]. The keto carbonyl group stretching frequency (1637 cm^{-1} in the free ligand) was slightly shifted due to an intramolecular hydrogen bond which was formed between phenolic group proton and oxygen of the keto carbonyl [21, 22]. The NH_2 bending of the ligand appeared at 661 cm^{-1} , which was shifted in complexes and appeared at $620\text{--}697\text{ cm}^{-1}$ due to coordination of amino nitrogen to metal ions [23–25].

Finally, the above interpretation was supported by the appearance of the new bands at $506\text{--}593$ and $450\text{--}488\text{ cm}^{-1}$ assigned to $\nu(M-O)$ and $\nu(M-N)$, respectively [7, 26]. Supporting that the bonding of the ligand to the metal ions was achieved by coordination of metal ions with one of the phenolic oxygen, amino and azomethine nitrogen atoms of the ligand so it behaved as neutral tridentate. These data will be supported by 1H NMR analysis [27].

3.4 1H NMR Spectrum

1H NMR spectral data (δ ppm) of the ligand proportionate to TMS (0 ppm) in $DMSO-d_6$. The signals observed at 9.83 and 12.22 ppm may be assigned to the phenolic OH^a and OH^b groups, respectively. The difference observed in these values may be due to estimated H-bonding linking the hydrogen atom of the $-OH$ group and the keto carbonyl group. These signals vanished in an existence of D_2O , indicating that these

Fig. 2 The full-scan mass spectra of **a** ligand and **b** Cr(III) complex **c** Ni(II) Complex



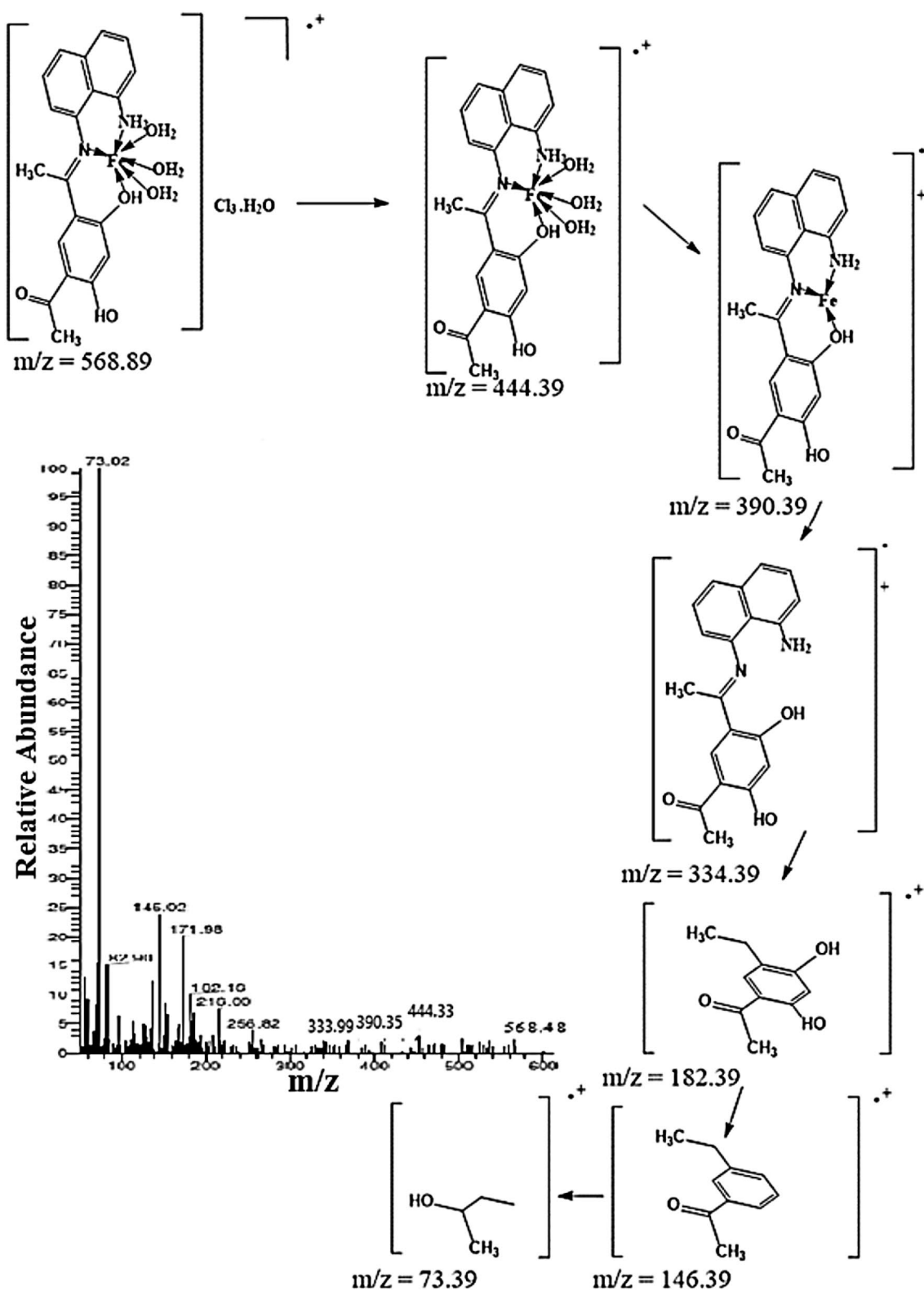


Fig. 3 Mass spectrum and fragmentation pattern of Fe(III) complex

protons are acidic and the phenolic groups can participate in the coordination with the metal ions [7, 27, 28]. The signal of the $-NH_2$ groups was found at 5.45 ppm and disappeared in presence of D_2O [27, 29]. The spectrum of free ligand (H_2L) exhibited a multiple signals in 7.05–6.39 ppm region which may be assigned to naphthalene protons (m, 6H) [28]. In the aromatic region, benzene shown as two singlet signals at 7.81 and 8.40 ppm [28].

1H NMR spectral data (δ ppm) of Zn(II) and Cd(II) complexes showed a down-field shift in the NH_2 resonance from δ 5.45 (free ligand) to 5.38 ppm (Zn(II) complex) and to 5.40 ppm (Cd(II) complex) indicating its coordination to the Zn(II) and Cd(II) ions, respectively [29]. The phenolic $-OH^a$ group showed its proton signal at 10.24 and 9.92 ppm in the Zn(II) and Cd(II) complexes, respectively, (9.83 ppm for H_2L ligand). These data confirmed that OH^a participated in coordination process without proton displacement. The other phenolic $-OH^b$ group not coordinating and still appeared in the same position as shown in the ligand spectrum [30, 31]. The singlet signal at 2.65 ppm corresponds to CH_3 protons of methyl moiety in the free Schiff base ligand was found at 2.88 and 2.89 for Cd(II) and Zn(II) complexes, respectively.

3.5 Molar Conductance Measurements

The molar conductance values of the complexes were measured at room temperature. These values showed that Zn(II) and Cd(II) complexes have no conductance and they were considered as nonelectrolytes. Cu(II), Cr(III), Mn(II), Co(II) and Ni(II) complexes had molar conductivity values of 52.0, 58.0, 60.0, 74.0 and 57.0 $\Omega^{-1} \text{ mol}^{-1} \text{ cm}^2$, respectively. These data suggest that these complexes are ionic in nature and they were electrolytes. The Fe(III) complex had a molar conductivity value of 139.5 $\Omega^{-1} \text{ mol}^{-1} \text{ cm}^2$, which suggested that this complex was ionic and electrolytic in nature in nature [9].

3.6 Electronic Spectral Study

It is possible to draw up the electronic transitions and foretell the geometry with the support of magnetic moments of most metal ions. The main absorption bands of the ligand were at 233, 276 and 324 nm and they were ascribed to $\pi \rightarrow \pi^*$ and $n \rightarrow \pi^*$ transitions within the aromatic rings in the ligand, respectively. The bands in all metal complexes located at 223–277 nm and 316–324 nm region were ascribed for $\pi \rightarrow \pi^*$ and $n \rightarrow \pi^*$ transitions, respectively, which can be related to the binding of these coordination centers to the central metal ions. The UV–vis spectra displayed bands at 537 nm which can be attributed to d–d transition in the Cr(III) complex [32, 33].

The electronic spectrum of Cr(III) complex showed three spin allowed bands at 18,150, 24,010 and 26,150 cm^{-1} .

These bands may be assigned to $^4A_{2g}(F) \rightarrow ^4T_{2g}(F)$, $^4A_{2g}(F) \rightarrow ^4T_{1g}(F)$ and $^4A_{2g}(F) \rightarrow ^4T_{1g}(P)$ transitions implying the octahedral geometry of the complex. The magnetic moment was found to be 3.98 B.M. which approved octahedral geometry of Cr(III) complex [34].

The Mn(II) complex showed three spin allowed bands at 17,280, 21,130 and 25,950 cm^{-1} . These bands may be assigned to $^4T_{1g} \rightarrow ^6A_{1g}$, $^4T_{2g}(G) \rightarrow ^6A_{1g}$ and $^4T_{1g}(D) \rightarrow ^6A_{1g}$ transitions implying the octahedral geometry of the complex. The measured magnetic moment was 5.64 B.M. which approved octahedral geometry of Mn(II) complex [9].

The Fe(III) complex showed three spin allowed bands at 22,460, 20,190 and 16,565 cm^{-1} . These bands may be assigned to $^4T_{2g}(G) \rightarrow ^6A_{1g}$, $^4T_{2g}(G) \rightarrow ^6A_{1g}$ and $^4T_{1g}(D) \rightarrow ^6A_{1g}$ transitions implying the octahedral geometry of the complex. The magnetic moment was 5.33 B.M. which approved octahedral geometry of Fe(III) complex [9, 35].

The Co(II) complex showed three spin allowed bands at 22,950, 20,110 and 16,245 cm^{-1} . These bands may be assigned to $^4T_{1g}(F) \rightarrow ^4T_{2g}(F)$, $^4T_{1g}(F) \rightarrow ^4A_{2g}(F)$ and $^4T_{1g}(F) \rightarrow ^4T_{2g}(P)$ transitions implying the octahedral geometry of the complex. The magnetic moment was calculated and found to be 4.89 B.M. which confirmed octahedral geometry of Co(II) complex [35].

The Ni(II) complex showed three spin allowed bands at 28,100, 22,185 and 11,970 cm^{-1} . These bands may be assigned to $^3A_{2g} \rightarrow ^3T_{1g}(P)$, $^3T_{1g}(P) \rightarrow ^3A_{2g}$ and $^3A_{2g}(F) \rightarrow ^3T_{1g}(F)$ transitions implying the octahedral geometry of the complex. The calculated magnetic moment was found to be 3.11 B.M. which pointed out the presence of octahedral Ni(II) complex [34, 35].

The Cu(II) complex showed three spin allowed bands at 21,016, 17,258 and 14,181 cm^{-1} which can be assigned to $^2B_{1g} \rightarrow ^2A_{1g}$, $^2B_{1g} \rightarrow ^2E_g$ and $^2B_{1g} \rightarrow ^2B_{2g}$ transitions, respectively, implying the octahedral geometry of the complex. The complex was found to has magnetic moment value of 2.09 B.M. which support its octahedral geometry [35, 36].

The Zn(II) and Cd(II) complexes were diamagnetic. According to the empirical formulae and an octahedral geometry for the Zn(II) and Cd(II) complexes was suggested [35].

3.7 Thermal Analysis

TG and DTG results of H_2L and its metal complexes at a heating rate of 10 $^\circ\text{C}/\text{min}$ in nitrogen atmosphere over the range from ambient temperature to 1000 $^\circ\text{C}$ were summarized in Table 1 [39].

The Schiff base ligand with the molecular formula ($C_{20}H_{18}N_2O_3$) was thermally decomposed in two successive decomposition steps within the range from 30 to 900 $^\circ\text{C}$ with total mass loss of 99.51% (calcd. 99.90%). The first step within the temperature range of 30–125 $^\circ\text{C}$ was correlated

Table 1 Thermoanalytical results (TG and DTG) of Schiff base ligand (H₂L) and its metal complexes

Complex	TG range (°C)	DTG _{max} (°C)	n*	Mass loss	Total mass loss Estim (Calcd) %	Assignment	Residues
H ₂ L	13–124	116	1	14.86 (14.35)	99.51 (99.9)	-Loss of CH ₆ NO	–
	124–758	233	1	84.65 (85.53)		-Loss of C ₁₉ H ₁₂ NO ₂	
[Cr(H ₂ L)(H ₂ O)Cl ₂]Cl·6H ₂ O	30–140	85	1	17.26 (17.45)	77.14 (77.95)	-Loss of 6H ₂ O	1/2Cr ₂ O ₃ + 5C
	140–300	230,265	2	20.33 (20.11)		-Loss of 3/2Cl ₂ , H ₂ O	
	300–900	350,845	2	39.55 (40.39)		-Loss of C ₁₅ H ₁₈ N ₂ O _{1.5}	
[Mn(H ₂ L)(H ₂ O) ₂]Cl·4H ₂ O	30–150	55,100,115	3	11.93 (12.67)	76.70 (77.59)	-Loss of 4H ₂ O	MnO + 6C
	150–250	205	1	21.01 (21.64)		-Loss of Cl ₂ , 2H ₂ O, CH ₄	
	250–900	275,460	2	43.76 (43.28)		-Loss of C ₁₄ H ₁₈ N ₂ O ₂	
[Fe(H ₂ L)(H ₂ O) ₃]Cl ₃ ·H ₂ O	30–300	200	1	24.8 (25.14)	74.53 (75.33)	-Loss of Cl ₂ , 4H ₂ O	1/2Fe ₂ O ₃ + 5C
	300–900	450,750	2	49.73 (50.19)		-Loss of 1/2Cl ₂ , C ₁₅ H ₁₈ N ₂ O _{1.5}	
[Co(H ₂ L)(H ₂ O) ₂]Cl·4H ₂ O	30–130	50,115	2	9.51 (9.43)	75.70 (76.34)	-Loss of 3H ₂ O	CoO + 5C
	130–350	160,250	2	21.06 (21.84)		-Loss of Cl ₂ , 3H ₂ O	
	350–900	650	1	45.13 (45.07)		-Loss of C ₁₅ H ₁₈ N ₂ O ₂	
[Ni(H ₂ L)(H ₂ O) ₂]Cl·6H ₂ O	30–100	60	1	11.73 (11.83)	75.99 (75.76)	-Loss of 4H ₂ O	NiO + 6C
	100–280	140,235	2	27.27 (26.13)		-Loss of Cl ₂ , 4H ₂ O, CH ₄	
	280–900	300,475,700	3	36.99 (37.8)		-Loss of C ₁₃ H ₁₄ N ₂ O ₂	
[Cu(H ₂ L)(H ₂ O) ₂]Cl·5H ₂ O	30–170	40,125	2	15.95 (15.13)	87.6 (86.64)	-Loss of 5H ₂ O	CuO
	170–235	200	1	5.69 (6.05)		-Loss of 2H ₂ O	
	235–700	300,375,500	3	65.96 (65.46)		-Loss of Cl ₂ , C ₂₀ H ₁₈ N ₂ O ₂	
[Zn(H ₂ L)(H ₂ O)Cl ₂]3H ₂ O	30–100	50	1	10.47 (9.96)	79.43 (78.36)	-Loss of 3H ₂ O	ZnO + 3C
	100–200	160	1	9.23 (9.86)		-Loss of H ₂ O, 1/2Cl ₂	
	200–350	275	1	10.23 (9.31)		-Loss of 1/2Cl ₂ , CH ₃	
	350–900	500,800	2	49.5 (49.23)		-Loss of C ₁₆ H ₁₅ N ₂ O ₂	
[Cd(H ₂ L)(H ₂ O)Cl ₂]	30–270	230	1	46.57 (46.1)	77.42 (76.52)	-Loss of Cl ₂ , H ₂ O, C ₁₀ H ₁₀ N ₂	CdO
	270–900	300,600,678,805	4	30.85 (30.42)		-Loss of C ₁₀ H ₁₁ O ₂	

with decomposition of CH₆NO molecule with mass loss of 14.86% (calcd. 14.35%) with a maximum at 116 °C. The second step within the temperature range of 125–760 °C which correlated with decomposition of C₁₉H₁₂NO₂ molecule with mass loss of 84.65% (calcd. 85.53%) with a maximum at 233 °C.

The [Cr(H₂L)(H₂O)Cl₂]Cl·6H₂O complex showed five decomposition steps within the range from 30 to 900 °C through total mass loss of 77.14% (calcd 77.95%) leaving 1/2Cr₂O₃ metal oxide contaminated by carbon atoms as residue. The first step within the temperature range of 30–140 °C was correlated by loss of six uncoordinated water molecules with mass loss of 17.26% (calcd. 17.45%) with a maximum at 85 °C. The second and third steps within the temperature range of 140–300 °C were correlated with loss of one coordinated water molecule and 3/2Cl₂ with mass loss of 20.33% (calculated mass loss = 20.11%) with two maxima at 230 and 265 °C. The last two steps within the temperature range of 300–900 °C were assigned to loss of C₁₅H₁₈N₂O_{1.5} molecule with mass loss of 39.55% (calcd. 40.39%) with two maxima at 350 and 845 °C.

The [Mn(H₂L)(H₂O)₂]Cl·4H₂O complex showed six decomposition steps within the temperature range from 30 to 900 °C with total mass loss of 76.70% (calcd. 77.59%) leaving MnO metal oxide contaminated by carbon atoms as residue. The first three steps within the temperature range of 30–150 °C were correlated with loss of four uncoordinated water molecules with mass loss of 11.93% (calcd. 12.67%) with a maximum at 55, 100 and 115 °C. The fourth step within the temperature range of 150–250 °C correlated by loss of Cl₂, 2H₂O and CH₄ molecules with mass loss of 21.01% (calcd. 21.64%) via a maximum at 205 °C. The last two steps within the temperature range of 250–900 °C were attributed to the loss of C₁₄H₁₈N₂O₂ molecule with mass loss of 43.76% (calcd. 43.28%) via two maxima at 275 and 460 °C.

The [Fe(H₂L)(H₂O)₃]Cl₃·H₂O complex showed three decomposition steps within the temperature range from 30 to 900 °C through total mass loss of 74.53% (calcd. 75.33%) leaving 1/2Fe₂O₃ contaminated by carbon atoms as residue. The first step within the temperature range of 30–300 °C can be accounted to the loss of Cl₂ and 4H₂O molecules

with mass loss of 24.8% (calcd. 25.14%) with a maximum at 200 °C. The last two steps within the temperature range of 300–900 °C were assigned to loss of $\frac{1}{2}\text{Cl}_2$ and $\text{C}_{15}\text{H}_{18}\text{N}_2\text{O}_{1.5}$ molecules with mass loss of 49.73% (calcd. 50.19%) with two maxima at 450 and 750 °C.

The $[\text{Co}(\text{H}_2\text{L})(\text{H}_2\text{O})_2\text{Cl}]\text{Cl}\cdot 4\text{H}_2\text{O}$ complex showed five decomposition steps within the temperature range from 30 to 900 °C through total mass loss of 75.70% (calcd. 76.34%) leaving CoO contaminated by carbon atoms as residue. The first and second steps within the temperature range of 30–130 °C were accounted to the loss of $3\text{H}_2\text{O}$ uncoordinated water molecules with mass loss of 9.51% (calcd. 9.43%) with a maximum at 50 and 115 °C. The third and fourth steps within the temperature range of 130–350 °C were assigned to loss of $3\text{H}_2\text{O}$ and Cl_2 molecules by mass loss of 21.06% (calcd. 21.84%) with a maximum at 160 and 250 °C. The last step within the temperature range of 350–900 °C correlated with loss of $\text{C}_{15}\text{H}_{18}\text{N}_2\text{O}_2$ molecule with mass loss of 45.13% (calcd. 45.07%) with maximum at 650 °C.

The $[\text{Ni}(\text{H}_2\text{L})(\text{H}_2\text{O})_2\text{Cl}]\text{Cl}\cdot 6\text{H}_2\text{O}$ complex showed six decomposition steps within the range from 30 to 900 °C with total mass loss of 75.99% (calcd. 75.76%) leaving NiO contaminated with carbon atoms as residue. The first step within the temperature range of 30–100 °C can correlated with loss of $4\text{H}_2\text{O}$ uncoordinated water molecules by mass loss of 11.73% (calcd. 11.83%) by a maximum at 60 °C. The second and third steps within the temperature range of 100–280 °C can assigned to the loss of $4\text{H}_2\text{O}$, Cl_2 and CH_4 molecules with mass loss of 27.27% (calcd. 26.13%) with maxima at 140 and 235 °C. The last three steps within the temperature range of 280–900 °C can accounted to the loss of $\text{C}_{13}\text{H}_{14}\text{N}_2\text{O}_2$ molecule by mass loss of 36.99% (calcd. 37.80%) with maxima at 300, 475 and 700 °C.

The $[\text{Cu}(\text{H}_2\text{L})(\text{H}_2\text{O})_2\text{Cl}]\text{Cl}\cdot 5\text{H}_2\text{O}$ complex showed six decomposition steps within the temperature range of 30–700 °C with total mass loss of 87.6% (calcd. 86.64%) leaving CuO as residue. The first and second steps within the temperature range of 30–170 °C can correlated with loss of $5\text{H}_2\text{O}$ hydrated water molecules with mass loss of 15.95% (calcd. 15.13%) via maxima at 40 and 125 °C. The third step within the temperature range of 170–235 °C was assigned to loss of $2\text{H}_2\text{O}$ molecules by mass loss of 5.69% (calcd. 6.05%) with a maximum at 200 °C. The last three steps within the temperature range of 235–700 °C can accounted to the loss of Cl_2 and $\text{C}_{20}\text{H}_{18}\text{N}_2\text{O}_2$ molecules by mass loss of 65.96% (calcd. 65.46%) with maxima at 300, 375 and 500 °C.

The $[\text{Zn}(\text{H}_2\text{L})(\text{H}_2\text{O})\text{Cl}_2]\cdot 3\text{H}_2\text{O}$ complex showed five decomposition steps within the temperature range of 30–900 °C with total mass loss of 79.43% (calcd. 78.36%) leaving ZnO contaminated by carbon atoms as residue. The first step within the temperature range of 30–100 °C can

correlated with loss of $3\text{H}_2\text{O}$ uncoordinated water molecules with mass loss of 10.47% (calcd. 9.96%) via a maximum at 50 °C. The second step within the temperature range of 100–200 °C can assigned to the loss of H_2O and $\frac{1}{2}\text{Cl}_2$ molecules by mass loss of 11.73% (calcd. 11.83%) with a maximum at 160 °C. The third step within the temperature range of 200–350 °C can accounted to the loss of $\frac{1}{2}\text{Cl}_2$ and CH_3 molecules with mass loss of 10.23% (calcd. 9.31%) with a maximum at 275 °C. The last two steps within the temperature range of 350–900 °C were assigned to the loss of $\text{C}_{16}\text{H}_{15}\text{N}_2\text{O}_2$ with mass loss of 49.5% (calcd. 49.23%) with two maxima at 500 and 800 °C.

The $[\text{Cd}(\text{H}_2\text{L})(\text{H}_2\text{O})\cdot\text{Cl}_2]$ complex showed five decomposition steps within the temperature range from 30 to 900 °C with total mass loss of 77.42% (calcd. 76.52%) leaving CdO as residue. The first step within the temperature range of 30–270 °C can correlated with the loss of H_2O , Cl_2 and $\text{C}_{10}\text{H}_{10}\text{N}_2$ molecules with mass loss of 46.57% (calcd. 46.10%) via a maximum at 230 °C. The last four steps within the temperature range of 270–900 °C can assigned to the loss of $\text{C}_{10}\text{H}_{11}\text{O}_2$ molecule with mass loss of 30.85% (calcd. 30.42%) with two maxima at 300, 600, 678 and 805 °C.

The thermograms of the complexes confirmed their structures where the presence of uncoordinated water molecules in all metal complexes except Cd(II) complex was suggested and all complexes have decomposed with three to six steps [39].

3.8 Geometry Optimization

The completely optimized geometries of the ligand H_2L and its Zn(II) complex were illustrated in Fig. 4. The values of the selected bond lengths and bond angles calculated for zinc(II) complex showed distorted octahedral geometry around the Zn(II) ion (Table 3). A slight elongation in bond lengths C5-N20, C11-N17, N20-C29 and O34-H35 was observed in the zinc(II) complex as ligand H_2L coordinated via azomethine nitrogen, amino nitrogen and phenolic oxygen. The Zn44-O34, Zn44-N20 and Zn44-N17 bond lengths were found to be 2.08, 2.20 and 2.17 Å, respectively. The four equatorial positions were occupied through azomethine nitrogen, amine nitrogen, phenolic oxygen and coordinated water oxygen while two axial positions were occupied by two chloride ions [8, 16].

3.8.1 Molecular Electrostatic Potential (MEP)

In order to study the reactions, electrostatic potential $V(r)$ maps were calculated which are known for the identification of the electronic charge distribution around molecular surface and subsequently to expect sites for the reactions.

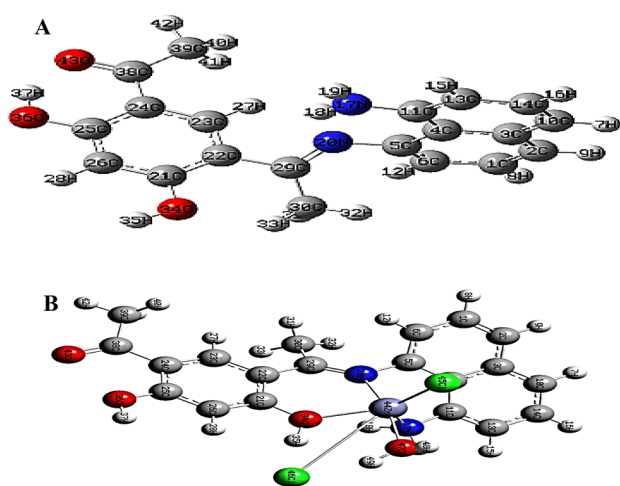


Fig. 4 The optimized structure of **a** H_2L and **b** its $Zn(II)$ complex

These maps were calculated by using the same basis set as for optimization. In the present study, 3D plots of MEP were drawn for the ligand and its $Zn(II)$ complex (Fig. 5). Based on the MEP, one can generally order the electron-rich area

which has red color on the map (favor site for electrophilic attack). However, the electron-poor region has blue color (favor site for nucleophilic attack). But the region with green color points to neutral electrostatic potential region. The H_2L is stable having approximately uniform distribution of charge density. However, oxygen and nitrogen atoms are surrounded with a greater negative charge surface, making these sites potentially more favorable for electrophilic attack (red) (Fig. 5). The aromatic ring seems neutral in terms of electron density. This distribution of potential is in favor of the complexation reaction which is further confirmed by electrostatic potential distribution of zinc(II) complex, where a greater negative charge is surrounded to the metal center (Fig. 5b). The Mulliken electronegativity also indicated the increase of electronegativity of oxygen and nitrogen in zinc(II) complex than free H_2L making them the favor site of electrophilic attack via metal ion. The charge of Zn atom decreased from (+2 to +0.67) due to coordination sphere process (Table 2) [16].

Fig. 5 Molecular electrostatic potential map of **a** H_2L and **b** $[Zn(H_2L)Cl_2]$. The electron density isosurface is 0.004 a.u

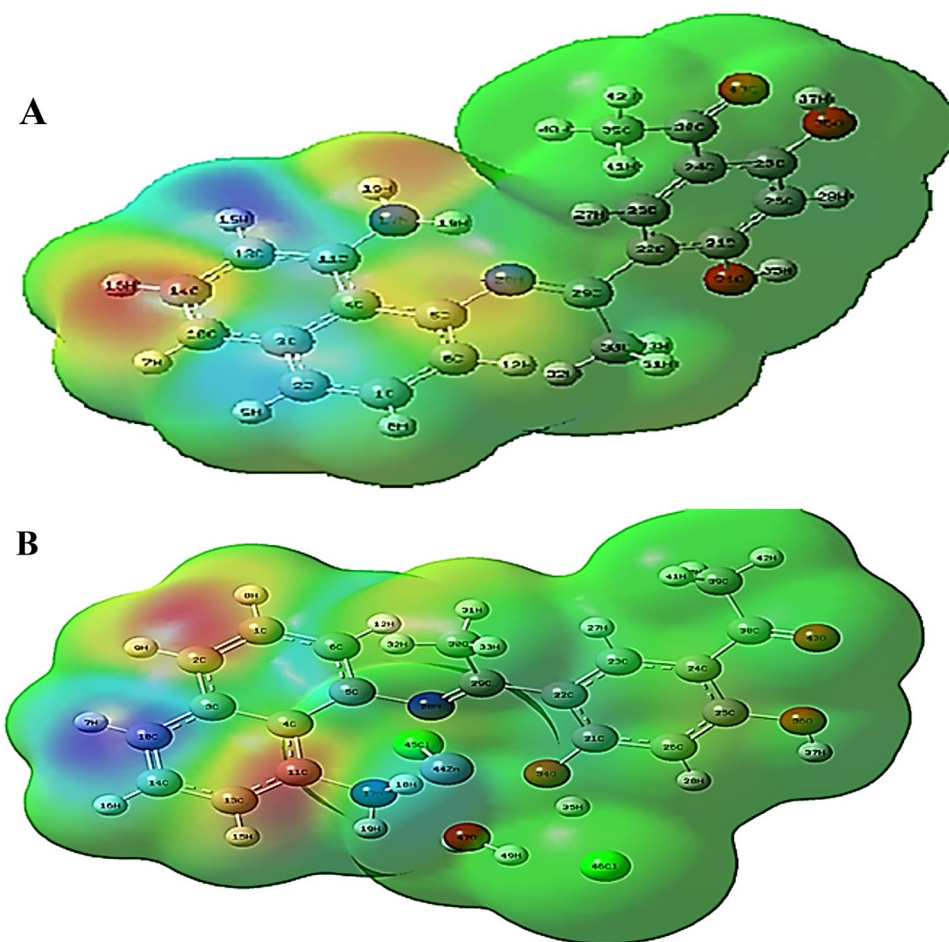


Table 2 The different Mulliken charges of H₂L and [Zn(H₂L)(H₂O)Cl₂]3H₂O complex

H ₂ L		[Zn(H ₂ L)(H ₂ O)Cl ₂]3H ₂ O	
Atom	Mulliken charge	Atom	Mulliken charge
C1	-0.128301	C1	-0.171426
C2	-0.213219	C2	-0.268762
C3	0.507019	C3	0.64741
C4	0.04668	C4	-0.197445
C5	0.066366	C5	0.304297
C6	-0.101049	C6	-0.12605
C10	-0.221732	C10	-0.305961
C11	0.151984	C11	0.090033
C13	-0.147299	C13	-0.166332
C14	-0.000285	C14	-0.030136
N17	-0.063033	N17	-0.087785
N20	0.046762	N20	-0.412205
C21	0.195427	C21	0.321537
C22	0.2407	C22	0.252224
C23	-0.195849	C23	-0.234237
C24	0.313713	C24	0.286018
C25	0.103192	C25	0.162136
C26	-0.254871	C26	-0.306877
C29	-0.051543	C29	0.104022
C30	0.074554	C30	-0.042803
O34	-0.130723	O34	-0.203246
O36	-0.075439	O36	-0.060497
C38	0.080901	C38	0.082708
C39	-0.016273	C39	-0.018823
O43	-0.227682	O43	-0.20927
		Zn44	0.67861
		Cl45	0.270471
		Cl46	-0.483585
		O47	0.12597

3.8.2 Molecular Parameters

Additional parameters such as the highest occupied molecular orbital energy (E_{HOMO}), the lowest unoccupied molecular orbital energy (E_{LUMO}), ΔE , absolute electronegativities, χ , chemical potentials, Π , absolute hardness, η , absolute softness, σ , global electrophilicity, ω , global softness, S , and additional electronic charge, ΔN_{max} have been estimated for the H₂L free ligand and its zinc(II) complex and registered in Table 3. Electrophilicity index (ω) is one of the greatest essential quantum chemical descriptors in describing toxicity and the reactivity of various selective sites. The electrophilicity may quantify the biological activity of drug receptor interaction. Also, this index measures the stabilization energy when the system acquires extra negative charge from the environment. η and σ indexes, are the measure of the molecular stability and

Table 3 The different optimized and quantum chemical parameters of H₂L and its zinc(II) complex

	H ₂ L	[Zn(H ₂ L)(H ₂ O)Cl ₂]3H ₂ O
Bond lengths (Å)		
C(4)–Cl(45)	–	4.15
C(5)–N(20)	1.42	1.44
C(11)–N(17)	1.39	1.46
C(11)–Cl(45)	–	4.35
N(17)–H(18)	1.01	1.02
N(17)–H(19)	1.00	1.02
N(17)–Zn(44)	–	2.17
N(20)–C(29)	1.30	1.32
N(20)–Zn(44)	–	2.20
C(21)–O(34)	1.39	1.38
O(34)–H(35)	0.98	1.06
O(34)–Zn(44)	–	2.08
Zn(44)–Cl(45)	–	2.32
Zn(44)–Cl(46)	–	4.07
Zn(44)–O(47)	–	2.11
O(47)–H(48)	–	0.98
O(47)–H(49)	–	1.00
Bond angles (°)		
Cl(45)–Zn(44)–Cl(46)	–	125.28
N(17)–Zn(44)–O(47)	–	90.11
N(20)–Zn(44)–O(34)	–	82.38
O(34)–Zn(44)–O(47)	–	86.98
N(17)–Zn(44)–N(20)	–	78.17
The calculated quantum chemical parameters		
E (a.u.)	-1108.00	-1280.09
Dipole moment (Debye)	2.18	10.55
E_{HOMO} (eV)	-5.04	-6.05
E_{LUMO} (eV)	-2.18	-2.28
ΔE (eV)	2.86	3.77
χ (eV)	3.61	4.17
η (eV)	1.43	1.89
σ (eV) ⁻¹	0.70	0.53
Π (eV)	-3.61	-4.17
S (eV) ⁻¹	0.35	0.26
ω (eV)	4.56	4.60
ΔN_{max}	2.52	2.21

reactivity. Also, their concepts are related to each other. The softness indexes are the vice versa image for global hardness. These parameters are useful in order to support the suggestion structures. The mentioned quantum chemical parameters were calculated with the help of the following equations: [16]

$$\Delta E = E_{LUMO} - E_{HOMO} \quad (1)$$

Table 4 Main calculated optical transition with composite ion in terms of molecular orbitals

Compound	Transition	Excitation energy (ev)	λ_{\max} Calc. (nm)	λ_{\max} exp. (nm)	Oscillating strength
H ₂ L	HOMO → LUMO+2	3.86	321	324	0.19
	HOMO → LUMO+4	4.49	276	276	0.02×10^{-1}
	HOMO → LUMO+5	5.34	232	233	0.02
[Zn(H ₂ L)(H ₂ O) Cl ₂]3H ₂ O	HOMO → LUMO+1	3.71	334	324	0.03
	HOMO- 10 → LUMO+1	5.42	228	226	0.03

Table 5 Biological activity of Schiff base ligand and metal complexes

	<i>Bacillus subtilis</i>	<i>Staphylococcus aureus</i>	<i>Escherichia coli</i>	<i>Pseudomonas aeruginosa</i>
Ligand H ₂ L	19	23	21	20
[Cr(H ₂ L)(H ₂ O) Cl ₂]Cl·6H ₂ O	16	15	16	17
[Mn(H ₂ L)(H ₂ O) ₂ Cl]Cl·4H ₂ O	17	14	14	17
[Fe(H ₂ L)(H ₂ O) ₃]Cl ₃ ·H ₂ O	16	15	15	16
[Co(H ₂ L)(H ₂ O) ₂ Cl]Cl·4H ₂ O	17	17	15	16
[Ni(H ₂ L)(H ₂ O) ₂ Cl]Cl·6H ₂ O	18	16	14	15
[Cu(H ₂ L)(H ₂ O) ₂ Cl]Cl·5H ₂ O	17	13	16	16
[Zn(H ₂ L)(H ₂ O) Cl ₂]3H ₂ O	13	14	12	14
[Cd(H ₂ L)(H ₂ O) Cl ₂]	18	16	16	20
Amikacin	10	9	6	10

$$\chi = \frac{-(E_{HOMO} + E_{LUMO})}{2} \quad (2)$$

$$\eta = \frac{E_{LUMO} - E_{HOMO}}{2} \quad (3)$$

$$\sigma = \frac{1}{\eta} \quad (4)$$

$$Pi = -\chi \quad (5)$$

$$S = \frac{1}{2\eta} \quad (6)$$

$$\omega = \frac{Pi^2}{2\eta} \quad (7)$$

$$\Delta N_{\max} = -\frac{Pi}{\eta} \quad (8)$$

The data calculated were presented in Table 4 and reflected the following notes:

1. The data of H₂L and its zinc(II) complex had a great chance and priority for biological activity based on high ω value.
2. S and ω were the softness indexes while η is for hardness indication; a hard molecule had a high stability due to its high energy difference in-between the E_{HOMO} and E_{LUMO} than the soft molecule. So, the soft molecule was the reactive one having flexible donation towards the metal ions. Accordingly, the investigated H₂L molecule was soft towards the coordination.
3. The positive electrophilicity index (χ) value and the negative electronic chemical potential (μ) value indicated that the H₂L molecule capable of accepting electrons from the environment and its energy must decrease upon accepting electronic charge. Therefore, the electronic chemical potential must be negative [16].
4. The Zn(II) complex showed high values of dipole moments than the free ligand.

Both the highest occupied molecular orbital (HOMO) and lowest unoccupied molecular orbital (LUMO) were the main orbitals that participate in chemical stability. The HOMO represents the ability to donate an electron, LUMO as an

electron acceptor represents the ability to obtain an electron. From the attained data (Table 5), it can assume that:

1. The energies of the HOMO and LUMO were negative values and more negative than free H_2L , which showed the stability of isolated complex.
2. The E_{HOMO} and E_{LUMO} values of zinc(II) complex were calculated and showed a decrease than the free ligand which represents the strength of $M-H_2L$ bonds.
3. The total energy of zinc(II) complex was higher than free ligand, which indicated greatly the stability of the isolated solid complex.
4. The small energy gap can be associated with a high chemical reactivity, low kinetic stability and reflects to efficient electronic charge transfer interaction making the molecule highly polarizable.
5. The HOMO level was mostly localized on the azomethine nitrogen and oxygen of phenol group in the ligand, which indicated the preferable sites for nucleophilic attack to the central metal atom [16].

3.8.3 UV–Vis Spectra

An interpretation of the photochemistry of transition metal compounds requires knowledge of the properties of molecular orbitals and appropriate excited states. Frontier orbitals played pertinent role in such systems, because they rule the electronic excitations and the transition characters. With the aid of TD-DFT calculations, it is possible to have comments about the contributions of the ligand and metal orbitals to molecular orbitals. It is not practical to analyze all the electronic transitions and the orbitals; therefore, some limitations were used. By reason of high accuracy and low computational cost of TD-DFT, it has been popularized for theoretical investigation of electronic spectra of molecules. The present exploration for low lying excited state on optimized ground state structures of H_2L and its zinc(II) complex have been performed at TD-DFT/B3LYP/LANL2DZ level of theory for thirty singlet state. In Table 5, the experimental and theoretical electronic spectra were presented. The TD-DFT calculations have been evaluated in the N,N-dimethyl-formamide solvent background and matched with the experimental data. The transitions between interfrontier

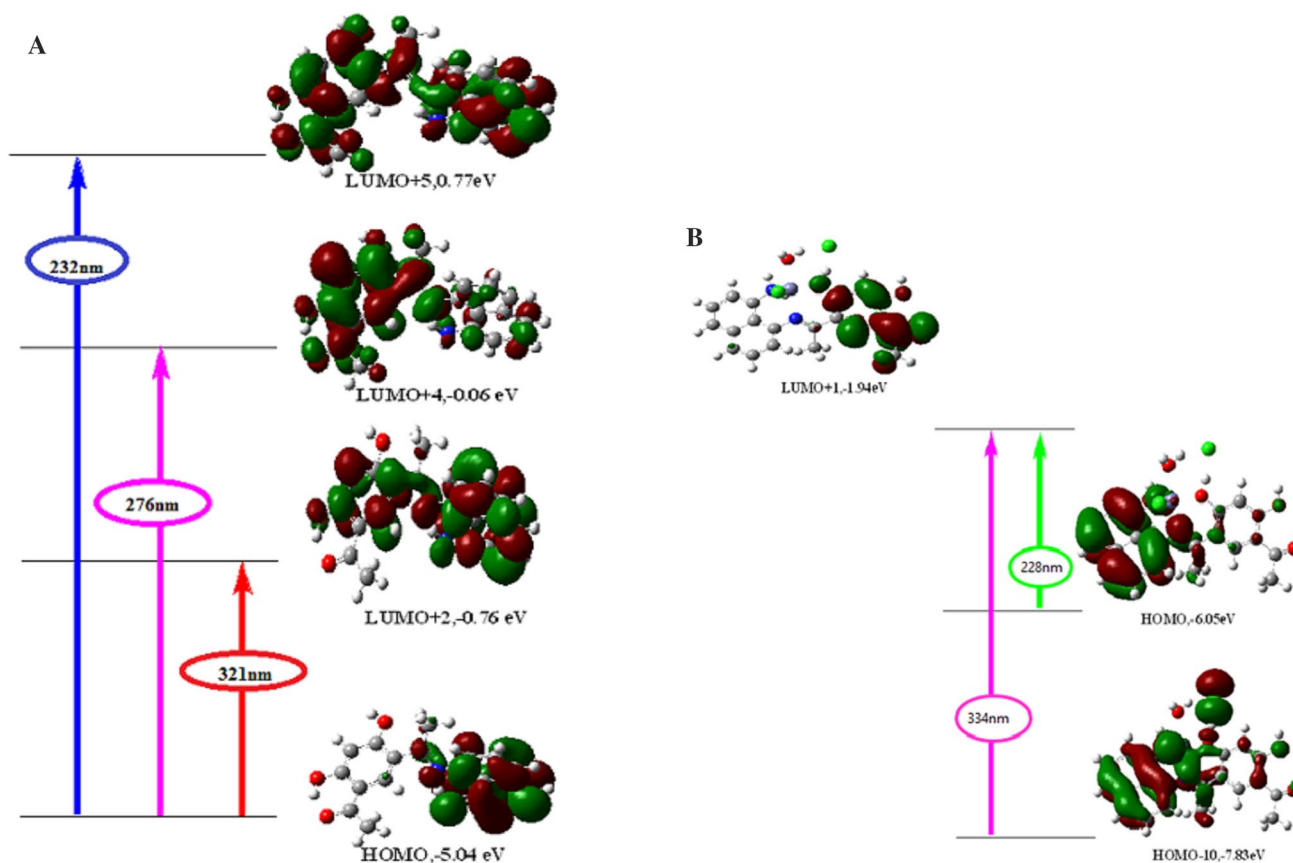


Fig. 6 **a** Theoretical electronic absorption transitions for H_2L in ethanol solvent. **b** Theoretical electronic absorption transitions for $Zn-H_2L$ complex in DMF solvent

orbitals for wavelengths corresponding to maximum oscillator strength of simulated results with contemporary experimental observations were presented in Fig. 6a, b. For example, the electronic transitions for H₂L obtained at calculated 321 nm correspond to experimental peak at 324 nm. This transition has been majorly contributed from HOMO to LUMO + 2 transitions which was primarily $n \rightarrow \pi^*$ in nature. The different transitions and its experimental counterpart of the free ligand and its zinc(II) complex have been summarized in Table 4 [16, 17].

3.9 Structural Interpretation

On the basis of the various physicochemical and spectral data presented and discussed above, the structures of the Cr(III), Mn(II), Fe(III), Co(II), Ni(II), Cu(II), Zn(II) and Cd(II) complexes were shown in Fig. 7.

3.10 Antimicrobial Activity

Antibacterial activity of H₂L ligand and Cr(III), Mn(II), Fe(III), Co(II), Ni(II), Cu(II), Zn(II) and Cd(II) complexes were tested against different bacterial species: two Gram(+) *Staphylococcus aureus* and *Bacillus subtilis* and two Gram(−) *Pseudomonas aeruginosa* and *Escherichia coli* by using modified agar diffusion method.

The results of antibacterial activity were tested in vitro as shown in Table 5. The metal complexes showed that the highest activity was found for Ni(II) and Cd(II) complexes against *Bacillus Subtilis* and the lowest activity against *Bacillus Subtilis* was observed for Zn(II) complex.

The Co(II) complex showed high activity while Cu(II) complex was the lowest active against *Staphylococcus aureus* [37].

The Cd(II), Cu(II) and Cr(III) complexes were highly active while Zn(II) complex was the lowest active against *Escherichia coli*.

The highly active was Cd(II) complex and the lowest active was Zn(II) complex against *Pseudomonas aeruginosa*.

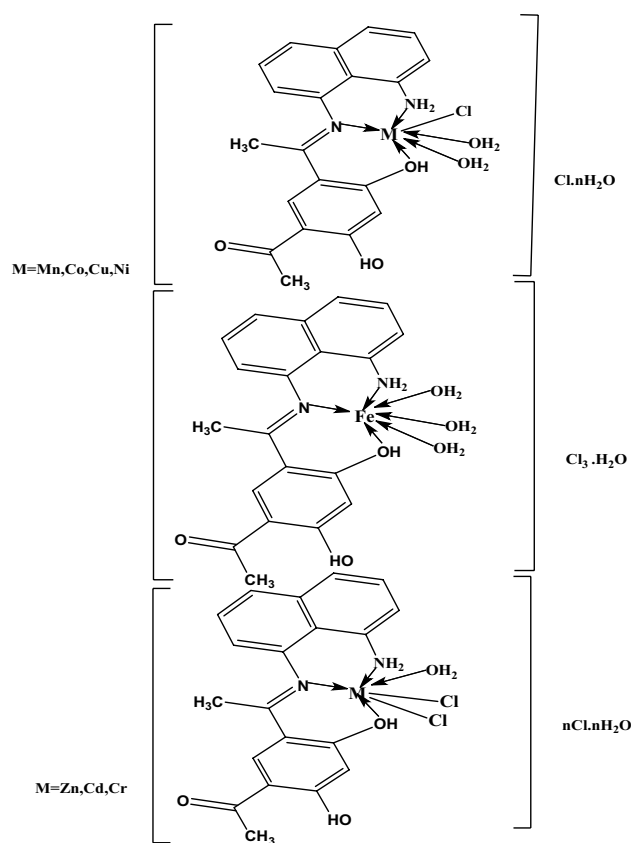


Fig. 7 Structures of metal complexes

The biological activity of these complexes was given graphically in Fig. 8.

3.11 Antitumor Activity

The in vitro anticancer activities of the synthesized Schiff base ligand and its complexes studied on human MCF-7 (breast cancer) cell line. The Ni(II), Cd(II), Mn(II) and Cu(II) complexes possess significant antitumor activity against MCF-7 proposing these compounds as potential

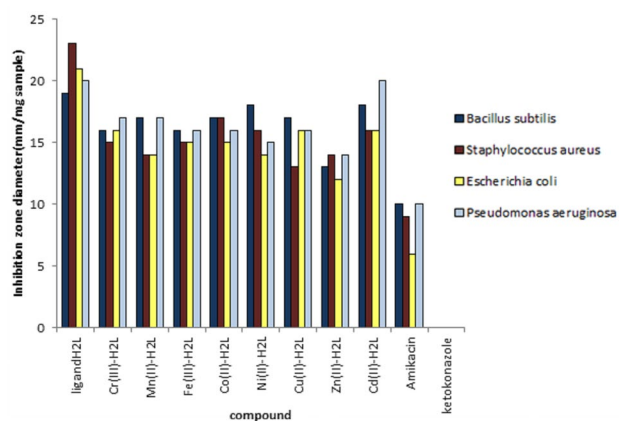


Fig. 8 Biological activity of Schiff base ligand and its metal complexes against different bacterial species

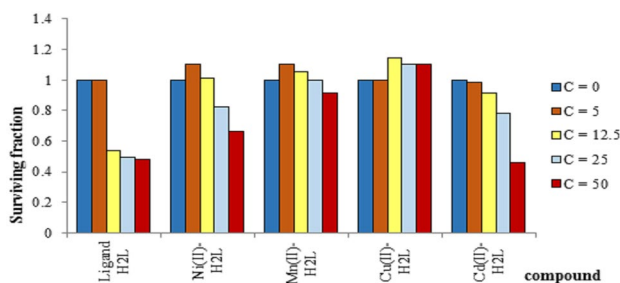


Fig. 9 Anticancer activity of Schiff base ligand (H_2L) and its metal complexes

antitumor agents (Fig. 9). It was believed that the ability of such compounds to inhibit tumor production was due to their chelating capability. The structure of the ligand and complexes played an important role in the anticancer activity. Thus, attachment of hydrophobic group in rigid ligands showed a better anticancer ability [8, 38, 39].

Negative BE

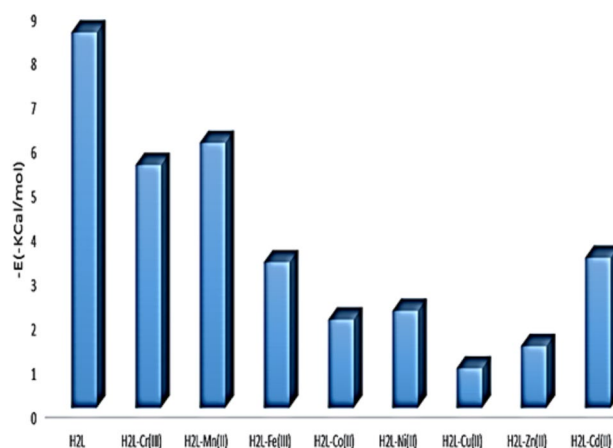


Fig. 10 The relation between the negative lowest binding energy of the ligand and their metal complexes with 3Q8U receptors

IC_{50} values of Ni(II), Cd(II) and ligand were found to be 50, 46 and 24.5 $\mu\text{g/ml}$, respectively. The Mn(II) and Cu(II) complexes need more than 50 $\mu\text{g/ml}$ to decrease validity of 50% of cancer cells. So the ligand had higher anticancer activity [38].

3.12 Molecular Docking Studies

Molecular docking analysis has been widely used to know the interactions of small drug molecules with bio targets like DNA and protein molecules. Additionally, binding site of the target specific region of the biomolecules can be predicted (Fig. 10) [39].

In the present study, 3Q8U was chosen as the model protein and the theoretical docking studies were demonstrated with Schiff base ligand and its metal complexes using patch dock web server tool [8]. One of the guides of molecular docking is to obtain an optimized conformation for each

Table 6 Energy values obtained in docking calculations of H₂L and there metal complexes with receptors Crystal structure of Staphylococcus aureus nucleoside diphosphate kinase complexed with ADP(3Q8U)

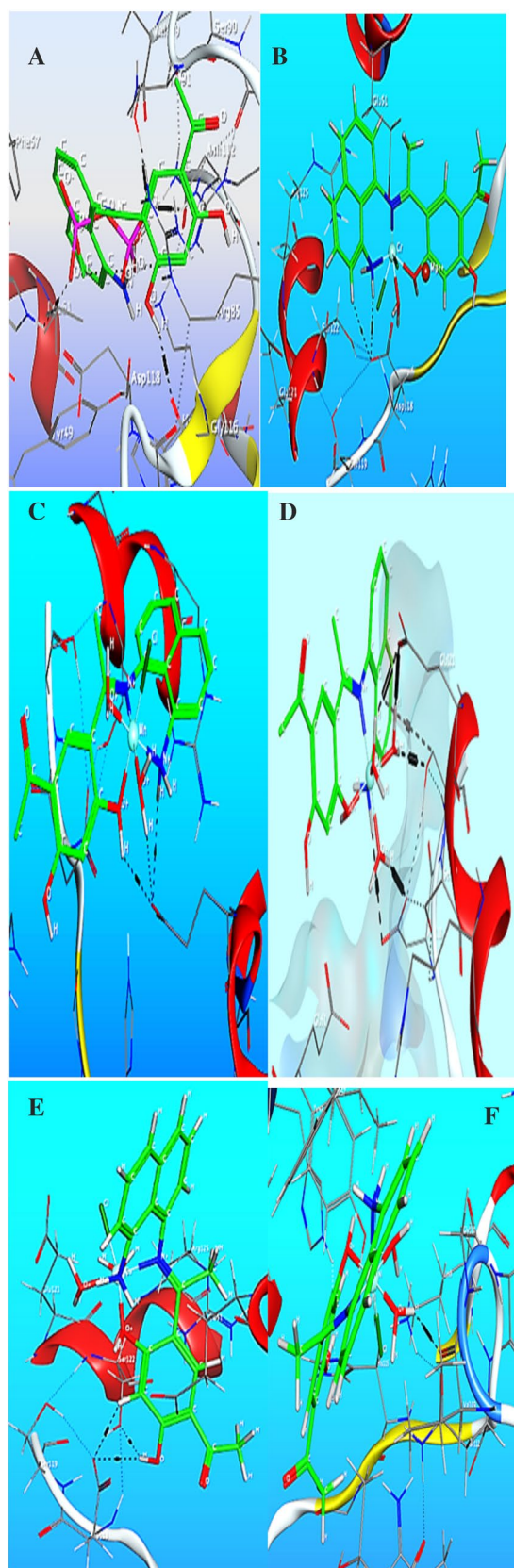
Compound	Moiety	Receptor site	Interaction	Distance (Å ^o)	E (kcal/mol)
Ligand	O43	NZ LYS 9	H-acceptor	2.90	– 8.5
[Co(H ₂ L)(H ₂ O) ₂ Cl] Cl·4H ₂ O	C26	OD2 ASP 118	H-donor	3.16	– 2
	O36	OD2 ASP 118	H-donor	3.05	– 0.7
	O36	OG SER 122	H-donor	3.14	– 0.6
	N17	OE1 GLU 51	Ionic	3.89	– 0.7
	O34	OE2 GLU 51	Ionic	3.78	– 1
	O45	OE1 GLU 121	Ionic	3.65	– 1.4
[Ni(H ₂ L)(H ₂ O) ₂ Cl] Cl·6H ₂ O	O45	O VAL 109	H-donor	2.43	– 2.2
[Cd(H ₂ L)Cl ₂ (H ₂ O)]	C26	OD2 ASP 118	H-donor	3.48	– 0.9
	O36	OD2 ASP 118	H-donor	3.25	– 0.7
	CL45	OE1 GLU 51	H-donor	3.40	– 0.5
	O46	OE1 GLU 121	H-donor	3.42	– 1.5
	O43	NH2 ARG 125	H-acceptor	2.81	– 3.4
	O46	OE1 GLU 121	Ionic	3.42	– 2.2
[Fe(H ₂ L)(H ₂ O) ₃] Cl ₃ ·H ₂ O	N17	OG1 THR 91	H-donor	3.12	– 3.3
	C39	OE2 GLU 51	H-donor	3.14	– 0.7
	O43	N ASP 118	H-acceptor	2.61	– 1.1
[Cr(H ₂ L)(H ₂ O)Cl ₂] Cl·6H ₂ O	C13	OD2 ASP	H-donor	3.37	– 1
	N17	OD2 ASP 118	H-donor	3.34	– 3.5
	CL44	OG SER 122	H-donor	2.28	0.7
	CL45	OE2 GLU 51	H-donor	2.91	0.4
	CL45	OD1 ASP 118	H-donor	2.49	5.4
	O43	NZ LYS 9	H-acceptor	3.07	– 2.9
	N17	OE2 GLU 51	Ionic	3.73	– 1.1
	N17	OD1 ASP 118	Ionic	3.44	– 2.1
	N17	OD2 ASP 118	Ionic	3.34	– 2.6
	N17	OE2 GLU 126	Ionic	3.02	– 4.3
	N20	OE2 GLU 51	Ionic	2.86	– 5.5
	N20	OE2 GLU 126	Ionic	3.63	– 1.4
	O34	OE2 GLU 126	Ionic	3.81	– 0.9
	O46	OD1 ASP 118	Ionic	3.24	– 3
	O46	OD2 ASP 118	Ionic	3.44	– 2.1
O46	OE2 GLU 126	Ionic	3.47	– 2	
[Mn(H ₂ L)(H ₂ O) ₂ Cl] Cl·4H ₂ O	N17	OE1 GLU 51	H-donor	2.82	– 0.8
	O34	OE1 GLU 51	H-donor	2.79	– 2.5
	N17	OE1 GLU 51	Ionic	2.82	– 5.8
	N17	OE2 GLU 51	Ionic	3.91	– 0.7
	O34	OE1 GLU 51	Ionic	2.79	– 6
	O34	OD1 ASP 118	Ionic	3.84	– 0.8
	O45	OE1 GLU 51	Ionic	3.54	– 1.7
[Zn(H ₂ L)(H ₂ O) Cl ₂] ₃ H ₂ O	C26	OD2 ASP 118	H-donor	3.26	– 1.4
	O36	OD2 ASP 118	H-donor	2.99	– 1.0
	O36	OG SER 122	H-donor	3.15	– 0.4
	CL46	OE1 GLU 51	H-donor	3.15	– 1.0
	O47	OE1 GLU 121	Ionic	3.91	– 0.7
[Cu(H ₂ L)(H ₂ O) ₂ Cl] Cl·5H ₂ O	N17	OG1 THR 91	H-donor	2.41	3.0
	6-ring	CA SER 90	Pi-H	4.43	– 0.9

Fig. 11 The interaction between H_2L and its metal complexes with receptor 3Q8U **a** H_2L , **b** $[Cr(H_2L)(H_2O)Cl_2]Cl \cdot 6H_2O$, **c** $[Mn(H_2L)(H_2O)_2Cl]Cl \cdot 4H_2O$, **d** $[Fe(H_2L)(H_2O)_3]Cl_3 \cdot H_2O$, **e** $[Co(H_2L)(H_2O)_2Cl]Cl \cdot 4H_2O$, **f** $[Ni(H_2L)(H_2O)_2Cl]Cl \cdot 6H_2O$, **g** $[Cu(H_2L)(H_2O)_2Cl]Cl \cdot 5H_2O$, **h** $[Zn(H_2L)(H_2O)Cl_2]3H_2O$, **i** $[Cd(H_2L)Cl_2(H_2O)]$

of the drug and protein with relative orientation between them such that the free energy of the overall system is minimized. The calculated structure of the Schiff base ligand and its metal complexes was docked with biological targets: the receptors of crystal structure of *Staphylococcus aureus* (PDB ID: 3Q8U). Also, the binding energies of the ligand and its metal complexes with receptors were calculated using computational docking studies. These energy values were listed in Table 6. The results showed that there are possible interactions between Schiff base ligand (H_2L) and its metal complexes with 3Q8U receptors. The docking results detected that the main interaction force of the Schiff base ligand with the active sites were H-acceptor. The lowest binding energies of the ligand and its metal complexes with 3Q8U receptors were calculated and the results represented graphically in Fig. 11. From the docking study for the ligand and its metal complexes, it was concluded that the ligand was favorably interacted with 3Q8U receptors. The strongest binding of H_2L with 3Q8U receptor, as it had the lowest binding energy value. By comparing the experimental and theoretical, it was found that H_2L had the highest activity with the lowest binding energy ($-8.50 \text{ kcal mol}^{-1}$) and the order of activity of other complexes was very near to the data obtained from experimental study [40–42].

4 Conclusions

Series of Cr(III), Mn(II), Fe(III), Co(II), Ni(II), Cu(II), Zn(II) and Cd(II) complexes were prepared with tridentate N,N and O donor novel Schiff base ligand (H_2L) resulted from the condensation of 4,6-diacetylresorcinol (4,6-DAR) with 1,8-naphth-alenediamine. They were characterized by various physicochemical techniques. The spectroscopic data showed that the Schiff base ligand acted in all metal complexes as neutral tridentate ligand through the azomethine nitrogen, amino nitrogen and the oxygen atom of phenolic group. Their molar conductivity values confirmed that Zn(II) and Cd(II) complexes were nonelectrolytes while Cr(III), Mn(II), Co(II), Cu(II) and Ni(II) were 1:1 electrolytes, while, Fe(III) complex was 1:2 electrolyte. The geometry of the complexes is assigned as octahedral. From the data of elemental analyses, the complexes have composition of the MH_2L type with general formula $[M(H_2L)(H_2O)_2Cl]$



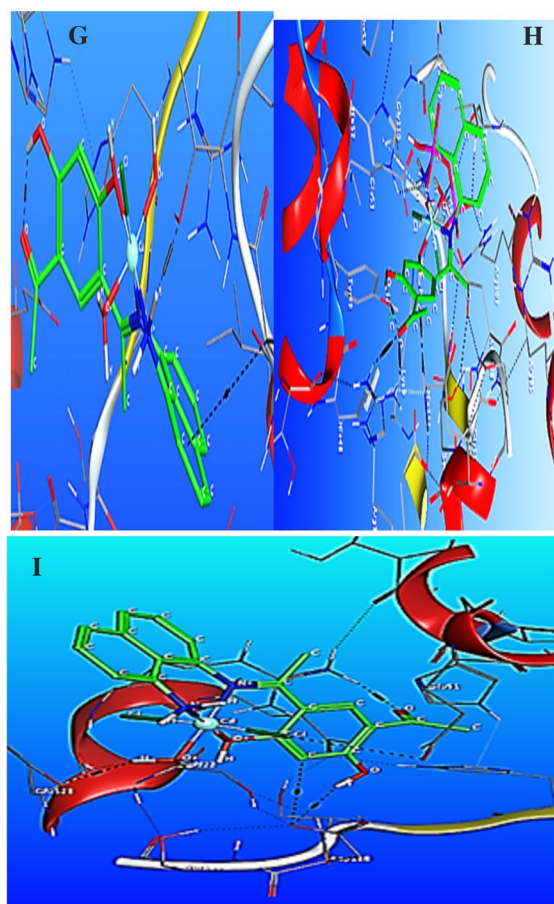


Fig. 11 (continued)

$\text{Cl}_n\text{H}_2\text{O}$ ($\text{M} = \text{Mn(II)}$ ($n = 4$), Co(II) ($n = 4$), Cu(II) ($n = 5$), Ni(II) ($n = 6$)), $[\text{M}(\text{H}_2\text{L})(\text{H}_2\text{O})\text{Cl}_2]_x\text{Cl}_n\text{H}_2\text{O}$ ($\text{M} = \text{Zn(II)}$ ($x = 0$, $n = 2$), Cd(II) ($x = 0$, $n = 0$), Cr(II) ($x = 1$, $n = 3$)), respectively, and $[\text{Fe(III)}(\text{H}_2\text{L})(\text{H}_2\text{O})_3]\text{Cl}_3$. The new complexes were subjected to study their biological potentials. The antimicrobial studies suggested that the Schiff base ligand and its metal complexes have significant biological activity. Hence, from all these extensive observations, it was concluded that the Schiff base ligand (H_2L) and its newly synthesized metal complexes give the remarkable, versatile and valuable information of coordination compounds and also, they may be used as good biological agents. The docking study showed that the H_2L and Mn(II) complex have the highest activity with the lowest binding energy of -8.50 and $-5.80 \text{ kcal mol}^{-1}$, respectively, and the order of activity of other complexes was very near to the data obtain from experimental study. The results of anticancer activities of the synthesized Schiff base ligand and its complexes studied on human MCF-7 (breast cancer) cell line showed that ligand, Cd(II) and Ni(II) complexes had higher anticancer activity. The DFT study showed that Zn(II) complex showed high values of dipole moments than the free ligand.

References

- M.B.A. Afonso, T.R. Cruz, Y.F. Silva et al., Ruthenium(II) complexes of Schiff base derived from cycloalkylamines as pre-catalysts for ROMP of norbornene and ATRP of methyl methacrylate. *J. Organomet. Chem.* **851**, 225–234 (2017)
- S. Malik, B. Jain, A.S. Mirza, A. Singh, Review study on metal complexes synthesized from therapeutically important Schiff. *Pharm. Chem. J.* **3**, 119–124 (2016)
- K. Brodowska, E. Łodyga-Chruścińska, Schiff bases—interesting range of applications in various fields of science. *Chemik* **68**, 129–134 (2014)
- M.Y. Nassar, T.Y. Mohamed, I.S. Ahmed, One-pot solvothermal synthesis of novel cobalt salicylaldehyde-urea complexes: a new approach to Co_3O_4 nanoparticles. *J. Mol. Struct.* **1050**, 81–87 (2013)
- M.Y. Nassar, H.M. Aly, M.E. Moustafa, E.A. Abdelrahman, Synthesis, characterization and biological activity of new and their Cu (II) complexes: a new approach to CuO nanoparticles for photocatalytic degradation of methylene blue. *J. Inorg. Organomet. Polym. Mater.* **27**, 1220–1233 (2017)
- W.H. Mahmoud, N.F. Mahmoud, G.G. Mohamed, New nanobidentate Schiff base ligand of 2-aminophenol with 2-acetyl ferrocene with some lanthanide metal ions: synthesis, characterization and Hepatitis A, B, C and breast cancer docking studies. *J. Coord. Chem.* **70**, 3552–3574 (2017)
- M. Shebl, M.A. El-Ghamry, S.M.E. Khalil, M.A.A. Kishk, Mono- and binuclear copper(II) complexes of new hydrazone ligands derived from 4,6-diacetylresorcinol: synthesis, spectral studies and antimicrobial activity. *Spectrochim. Acta Part A Mol. Biomol. Spectrosc.* **126**, 232–241 (2014)
- K. Dhahagani, M.P. Kesavan, G. Gangatharan et al., Crystal structure, optical properties, DFT analysis of new morpholine based Schiff base ligands and their copper(II) complexes: DNA, protein docking analyses, antibacterial study and anticancer evaluation. *Mater. Sci. Eng. C.* **1**(90), 119–130 (2018)
- W.H. Mahmoud, R.G. Deghadi, G.G. Mohamed, Novel Schiff base ligand and its metal complexes with some transition elements. Synthesis, spectroscopic, thermal analysis, antimicrobial and in vitro anticancer activity. *Appl. Organomet. Chem.* **30**, 221–230 (2016)
- A.W. Bauer, W.M. Kirby, C. Sherris, M. Turck, Antibiotic susceptibility testing by a standardized single disk method. *Am. J. Clin. Pathol.* **45**, 493–496 (1966)
- L.D. Liebowitz, H.R. Ashbee, E.G. Evans, Y. Chong, N. Mallatova, M. Zaidi, D. Gibbs, Global Antifungal Surveillance Group, a two year global evaluation of the susceptibility of *Candida* species to fluconazole by disk diffusion. *Diagn. Microbiol. Infect.* **40**, 27–33 (2001)
- J.C. Chang, P.R. Hsueh, J.J. Wu, S.W. Ho, W.C. Hsieh, K.T. Luh, Antimicrobial susceptibility of flavobacteria as determined by agar dilution and disk diffusion methods. *Antimicrob. Agents Chemother.* **41**, 1301–1306 (1997)
- Pa. Villanova, National Committee for Clinical Laboratory Standards. Methods for dilution antimicrobial susceptibility tests for bacteria that grow aerobically. Approved standard M7-A3. National Committee for Clinical Laboratory Standards (1993)
- M.J. Matar, L. Ostrosky-Zeichner, V.L. Paetznick, J.R. Rodriguez, E. Chen, J.H. Rex, Correlation between E-test, disk diffusion, and microdilution methods for antifungal susceptibility testing of fluconazole and voriconazole. *Antimicrob. Agents Chemother.* **47**, 1647–1651 (2003)
- P. Skehan, R. Storeng, D. Scudiero, A. Monks, J. McMahon, D. Vistica, J.T. Warren, H. Bokesch, S. Kenney, M.R. Boyd, New

- colorimetric cytotoxicity assay for anti-cancer-drug screening. *J. Natl. Cancer Inst.* **82**, 1107 (1990)
16. W.H. Mahmoud, G.G. Mohamed, O.Y. El-Sayed, Coordination compounds of some transition metal ions with new Schiff base ligand derived from dibenzoyl methane. Structural characterization, thermal behavior, molecular structure, antimicrobial, anticancer activity and molecular docking studies. *Appl. Organomet. Chem.* **32**, e4051 (2017)
 17. M.N. Ibrahim, S.A.I. Sharif, Synthesis, characterization and use of Schiff bases as fluorimetric analytical reagents (Part II). *E-J. Chem.* **8**, 180–184 (2011)
 18. L.H. Abdel-rahman, N.M. Ismail, M. Ismael, A.M. Abu-dief, E.A. Ahmed, Synthesis, characterization, DFT calculations and biological studies of Mn (II), Fe (II), Co (II) and Cd (II) complexes based on a tetradentate ONNO donor Schiff base ligand. *J Mol Struct.* **1134**, 851–862 (2017)
 19. M.R. Maurya, L. Rana, F. Avecilla, Phloroglucinol and resorcinol based mononuclear dioxidomolybdenum(VI) complexes: synthesis, structural characterization and catalytic epoxidation. *Polyhedron* **126**, 60–71 (2017)
 20. A.B. Deilami, M. Salehi, A. Arab, A. Amiri, Synthesis, crystal structure, electrochemical properties and DFT calculations of three new Zn (II), Ni (II) and Co (III) complexes based on. *Inorg. Chim. Acta.* **476**, 93–100 (2018)
 21. M.L. Smith, K.G. Paul, Infrared spectroscopic evidence of hydrogen bonding between carbon monoxide and protein in carbonylhorseradish peroxidase C. *FEBS Lett.* **163**, 303–305 (1983)
 22. M. Jafari-moghaddam, S.A. Beyramabadi, M. Khashi, A. Morsali, Three VO^{2+} complexes of the pyridoxal-derived Schiff bases: synthesis, experimental and theoretical characterizations, and catalytic activity in a cyclocondensation reaction. *J. Mol. Struct.* **1153**, 149–156 (2017)
 23. Y. Liu, J. Sheng, D. Yin et al., Ferrocenyl chalcone-based Schiff bases and their metal complexes: highly efficient, solvent-free synthesis, characterization, biological research. *J. Organomet. Chem.* **856**, 27–33 (2018)
 24. R. Katava, M. Rajic, G. Pavlovic, On the zinc (II) and mercury (II) compounds with Schiff-base N-(p-anisoyl)-2-oxo-1-naphthylideneamine Tautomerism of the ligand and polymerization of mercury compound via Hg...I contact. *Polyhedron* **123**, 285–292 (2017)
 25. W.H. Mahmoud, N.F. Mahmoud, G.G. Mohamed, Spectroscopic characterization and molecular docking studies of acetyl ferrocene-derived Schiff base ligand with phenanthroline and some transition metal ions. *J. Therm. Anal. Calorim.* **131**, 2775–2793 (2017)
 26. E. Yousif, A. Majeed, K. Al-Sammarae, N. Salih, J. Salimon, B. Abdullah, Metal complexes of Schiff base: preparation, characterization and antibacterial activity. *Arab. J. Chem.* **10**, 1639–S1644 (2017)
 27. A.A.A. Emara, O.M.I. Adly, Synthesis and spectroscopic studies of new binuclear transition metal complexes of Schiff bases derived from 4,6-diacetylresorcinol. *Transit Met. Chem.* **32**, 889–901 (2007)
 28. J.H. Pandya, R.N. Jadeja, K.J. Ganatra, Spectral characterization and biological evaluation of Schiff bases and their mixed ligand metal complexes derived from 4,6-diacetylresorcinol. *J. Saudi Chem. Soc.* **18**, 190–199 (2014)
 29. E.S. Aazam, M.P. Coles, Simple generation of neutral bimetallic aluminium and zinc alkyls Schiff bases bridged by a central resorcinol moiety. *Cent. Eur. J. Chem.* **8**, 1305–1310 (2010)
 30. M. Shakir, M. Azam, M.F. Ullah, S.M. Hadi, Synthesis, spectroscopic and electrochemical studies of N, N-bis[(E)-2-thienylmethylidene]-1,8-naphthalenediamine and its Cu(II) complex: DNA cleavage and generation of superoxide anion. *J. Photochem. Photobiol. B Biol.* **104**, 449–456 (2011)
 31. P. Tyagi, M. Tyagi, S. Agrawal, S. Chandra, H. Ojha, M. Pathak, Synthesis, characterization of 1, 2, 4-triazole Schiff base derived 3d-metal complexes: induces cytotoxicity in HepG2, MCF-7 cell line, BSA binding fluorescence and DFT study. *Spectrochim. Acta Part A Mol. Biomol. Spectrosc.* **171**, 246–257 (2017)
 32. A.A.A. Abou-Hussein, W. Linert, Synthesis, spectroscopic and biological activities studies of acyclic and macrocyclic mono and binuclear metal complexes containing a hard-soft Schiff base. *Spectrochim. Acta Part A Mol. Biomol. Spectrosc.* **95**, 596–609 (2012)
 33. W.H. Mahmoud, R.G. Deghadi, G.G. Mohamed, Preparation, geometric structure, molecular docking thermal and spectroscopic characterization of novel Schiff base ligand and its metal chelates: screening their anticancer and antimicrobial activities. *J. Therm. Anal. Calorim.* **127**, 2149–2171 (2017)
 34. C.E. Housecroft, A.G. Sharpe, *Inorganic Chemistry* (Third, Pearson Education, 2008)
 35. W.H. Mahmoud, F.N. Sayed, G.G. Mohamed, Synthesis, characterization and *in vitro* antimicrobial and anti-breast cancer activity studies of metal complexes of novel pentadentate azo dye ligand. *Appl. Organomet. Chem.* **30**, 959–973 (2016)
 36. A. Thakar, K. Joshi, K. Pandya, A. Pancholi, Coordination modes of a Schiff Base derived from substituted 2-aminothiazole with chromium(III), manganese(II), iron(II), cobalt(II), nickel(II) and copper(II) metal ions : synthesis spectroscopic and antimicrobial studies. *J. Chem.* **8**, 1750–1764 (2011)
 37. S.K. Tadavi, A.A. Yadav, R.S. Bendre, Synthesis and characterization of a novel schiff base of 1,2-diaminopropane with substituted salicylaldehyde and its transition metal complexes: Single crystal structures and biological activities. *J. Mol. Struct.* **1152**, 223–231 (2017)
 38. B. Assay, S. Base, B. Iftikhar et al., Synthesis, characterization and biological assay of salicylaldehyde Schiff Base Cu(II) complexes and their precursors. *J Mol Struct.* **1155**, 337–348 (2017)
 39. W.H. Mahmoud, M.M. Omar, Y.M. Ahmed, G.G. Mohamed, Transition metal complexes of Schiff base ligand based on 4,6-diacetyl resorcinol. *Appl. Organomet. Chem.* **34**, 1–20 (2020)
 40. W.H. Mahmoud, R.G. Deghadi, G.G. Mohamed, Metal complexes of novel Schiff base derived from iron sandwiched organometallic and 4-nitro-1,2-phenylenediamine: synthesis, characterization, DFT studies, antimicrobial activities and molecular docking. *Appl. Organomet. Chem.* **32**, e4289 (2018)
 41. N.S. Al-Radadi, E.M. Zayed, G.G. Mohamed, H.A. Abd El Salam, Synthesis, spectroscopic characterization, molecular docking, and evaluation of antibacterial potential of transition metal complexes obtained using triazole chelating ligand. *J. Chem.* **1548641**, 1–12 (2020)
 42. R.G. Deghadi, W.H. Mahmoud, G.G. Mohamed, Metal complexes of tetradentate azo-dye ligand derived from 4,4'-oxydianiline: preparation, structural investigation, biological evaluation and MOE studies. *Appl. Organomet. Chem.* **34**, 1–20 (2020)